

# 1 The Paleocene-Eocene Thermal Maximum at DSDP Site 2 277, Campbell Plateau, southern Pacific Ocean

3  
4 C. J. Hollis<sup>1</sup>, B. R. Hines<sup>2</sup>, K. Littler<sup>3,4</sup>, V. Villasante-Marcos<sup>5</sup>, D. K. Kulhanek<sup>6</sup>, C.  
5 P. Strong<sup>1</sup>, J. C. Zachos<sup>3</sup>, S. M. Eggins<sup>7</sup>, L. Northcote<sup>8</sup> and A. Phillips<sup>1</sup>

6  
7 [1] {GNS Science, Lower Hutt, New Zealand}

8 [2] {School of Geography, Environment & Earth Sciences, Victoria University of  
9 Wellington, New Zealand}

10 [3] {Earth & Planetary Sciences, University of California – Santa Cruz, California, United  
11 States}

12 [4] {Camborne School of Mines, University of Exeter, Penryn Campus, Cornwall, United  
13 Kingdom}

14 [5] {Observatorio Geofísico Central, Instituto Geográfico Nacional, Madrid, Spain}

15 [6] {International Ocean Discovery Program, Texas A&M University, College Station,  
16 Texas, United States}

17 [7] {Research School of Earth Sciences, The Australian National University, Canberra, ACT,  
18 Australia}

19 [8] {National Institute of Water and Atmosphere, Wellington, New Zealand}

20 Correspondence to: C. J. Hollis (c.hollis@gns.cri.nz)

## 21 22 **Abstract**

23 Re-examination of sediment cores from Deep Sea Drilling Project (DSDP) Site 277 on the  
24 western margin of the Campbell Plateau (paleolatitude of ~65°S) has identified an intact  
25 Paleocene-Eocene (P-E) boundary overlain by a 34 cm-thick record of the Paleocene-Eocene  
26 Thermal Maximum (PETM) within nanofossil chalk. The upper part of the PETM is  
27 truncated, either due to drilling disturbance or a sedimentary hiatus. An intact record of the  
28 onset of the PETM is indicated by a gradual decrease in  $\delta^{13}\text{C}$  values over 20 cm, followed by  
29 a 14 cm interval in which  $\delta^{13}\text{C}$  is 2‰ lighter than uppermost Paleocene values. After  
30 accounting for effects of diagenetic alteration, we use  $\delta^{18}\text{O}$  and Mg/Ca values from  
31 foraminiferal tests to determine that intermediate and surface waters warmed by ~5-6° at the  
32 onset of the PETM prior to the full development of the negative  $\delta^{13}\text{C}$  excursion. After this

33 initial warming, sea temperatures were relatively stable through the PETM, but declined  
34 abruptly across the horizon that truncates the event at this site. Mg/Ca analysis of  
35 foraminiferal tests indicate peak intermediate and surface water temperatures of ~19°C and  
36 ~32°C, respectively. These temperatures may be influenced by residual diagenetic factors,  
37 changes in ocean circulation, and surface water values may also be biased towards warm  
38 season temperatures.

39

## 40 **1 Introduction**

41 Stable isotope analysis of foraminiferal tests from sediments cored at DSDP Site 277  
42 (Shackleton and Kennett, 1975) provided the first paleotemperature record for the Paleogene  
43 of the Southern Ocean and laid the foundation for many subsequent studies of the regional  
44 paleoclimate and paleoceanography (e.g., Kennett 1977, 1980; Kennett and Shackleton,  
45 1976; Hornibrook, 1992; Nelson and Cook, 2001). Over the last decade, there has been  
46 renewed interest in the early Paleogene (66 to 35 Ma) climate history of the Southern Ocean,  
47 partly driven by a societal imperative to understand how the Antarctic ice sheet will respond  
48 to anthropogenic global warming (e.g., Joughin et al., 2014). The early Paleogene was the  
49 last time that Earth is inferred to have experienced greenhouse gas levels in excess of ~600  
50 ppm CO<sub>2</sub> (Zachos et al., 2008; Beerling and Royer, 2011), and therefore provides insight into  
51 a climate state that civilization may experience in coming centuries. One event in particular  
52 has been touted as a geological analogue for greenhouse gas-driven global warming: the  
53 Paleocene-Eocene Thermal Maximum (PETM, ~56 Ma). This event was a short-lived (~220  
54 kyrs) perturbation to the climate and carbon cycle in which global temperatures rose by 4–  
55 5°C within a few thousand years (Sluijs et al., 2007; McInerney and Wing, 2011; Dunkley-  
56 Jones et al., 2013; Schmidt, 2014), with warming of up to 8°C in higher latitudes and some  
57 coastal settings (Thomas et al., 2002; Sluijs et al., 2006, 2011; Zachos et al., 2006; Hollis et  
58 al., 2012; Frieling et al., 2014). Multiple lines of evidence suggest that this warming may  
59 have been driven by a rapid injection of greenhouse gases, possibly sourced from submarine  
60 gas hydrates, as evidenced by coupled negative excursions in oxygen and carbon isotopes  
61 (Dickens et al., 1995, 1997). Several other potential sources of the light carbon have also  
62 been implicated to account for all or part of the carbon isotope ( $\delta^{13}\text{C}$ ) excursion (Dickens,  
63 2003, 2011; Kent et al., 2003; Svensen et al., 2004; Higgins and Schrag, 2006; De Conto et  
64 al., 2012).

65

66 The PETM has been identified in several sites in the Southwest Pacific, including onshore  
67 records in both siliciclastic and pelagic bathyal sections in eastern New Zealand (Kaiho et al.,  
68 1996; Crouch et al., 2001; Hancock et al., 2003; Hollis et al., 2005a, b, 2012; Nicolo et al.,  
69 2010), non-marine to marginal marine sediments in western New Zealand (Handley et al.,  
70 2011) and in shelfal sediments at Ocean Drilling Program (ODP) Site 1172, offshore eastern  
71 Tasmania (Sluijs et al., 2011). Here we report a new record of the PETM in pelagic bathyal  
72 sediments at DSDP Site 277, at a similar paleolatitude to Site 1172 (~65°S). These two sites  
73 represent the southernmost records of the PETM in the Pacific Ocean (Fig. 1).

74 Initial studies of Site 277 suggested that the Paleocene-Eocene (P-E) boundary occurred  
75 within a gap between cores 43 and 44 (Kennett et al., 1975). A subsequent biostratigraphic  
76 review of the site (Hollis et al., 1997) revealed that the boundary was lower in the drillhole,  
77 potentially within a relatively continuous interval preserved in core 45. Detailed re-sampling  
78 confirmed the location of the P-E boundary (Fig. 2), based on the highest occurrence (HO) of  
79 benthic foraminifer *Stensionina beccariformis* at 457.3 mbsf (277-45-3, 80 cm). High  
80 resolution stable isotope analysis of bulk carbonate confirms that this horizon marks the base  
81 of a 34 cm-thick negative excursion in  $\delta^{13}\text{C}$  (CIE) that defines the PETM (Aubry et al.,  
82 2007).

83 DSDP Site 277 was drilled on the western margin of the Campbell Plateau in a water depth of  
84 1214 m as part of DSDP Leg 29 (Kennett et al., 1975). Paleogene sedimentation occurred in  
85 fully oceanic conditions well above the lysocline (Kennett et al., 1975), with benthic  
86 foraminiferal assemblages indicating lower to middle bathyal water depths since the  
87 Paleocene (Hollis et al., 1997). In order to identify the paleoceanographic changes associated  
88 with the PETM at this site we have undertaken a multidisciplinary study that includes  
89 foraminiferal and calcareous nannofossil biostratigraphy, magnetic susceptibility,  $\text{CaCO}_3$   
90 content, elemental abundance using X-ray fluorescence (XRF),  $\delta^{13}\text{C}$  and  $\delta^{18}\text{O}$  analysis of  
91 bulk carbonate and foraminifera, and single test analysis of foraminifera for Mg/Ca ratios by  
92 Laser Ablation Inductively Coupled Plasma Mass Spectrometry (LA-ICPMS).

93

## 94 **2 Material and Methods**

### 95 **2.1 Material**

96 We analysed samples over a 45-m interval spanning the upper Paleocene to lower Eocene at  
97 DSDP Site 277 (470–425 mbsf). Average sample spacing was 20 cm over much of the  
98 interval, with a higher resolution of 2–3 cm sampling across the PETM within core-section  
99 45-3 (~457.30–456.95 mbsf). In addition, this core-section was scanned for elemental  
100 abundance. Although the PETM interval is preserved, the overall record is discontinuous,  
101 with significant gaps between cores from core 42 to 45 (Fig. 2).

102

### 103 **2.2 Methods**

#### 104 **2.2.1 X-Ray fluorescence (XRF) core scanning**

105 XRF data were acquired using an Avaatech XRF scanner with a Canberra X-PIPS silicon  
106 drift detector, model SXD 15C-150-500 150 eV resolution X-ray detector, which is housed at  
107 the International Ocean Discovery Program (IODP) Gulf Coast Repository at Texas A&M  
108 University in College Station, Texas (Table S1). This scanner is configured for analysis of  
109 split core section halves, with the X-ray tube and detector mounted on a moving track  
110 (Richter et al., 2006). Section 277-45-3 was removed from the core refrigerator and allowed  
111 to equilibrate to room temperature prior to analysis. We levelled all rock pieces within the  
112 section, as the detector requires a flush surface with no gaps between pieces, and then  
113 covered the section with 4 µm thick Ultralene plastic film (SPEX Centriprep, Inc.) to protect  
114 the detector. The section was scanned at 2 mm intervals using a voltage of 10 kV for  
115 elements Al, Si, P, S, Cl, Ar, K, Ca, Ti, Cr, Mn, Fe, Rh, and Ba. The scan was completed  
116 using a 1 mA tube current, no filter, and a detector live time of 30 s, with an X-ray detection  
117 area of 2 mm in the downcore direction and 15 mm across the core. During measurement,  
118 intervals were skipped where gaps of more than ~2 mm existed between pieces. Smaller gaps  
119 were noted so that suspect data across these gaps could be removed.

#### 120 **2.2.2 Rock magnetism**

121 Bulk magnetic susceptibility of a subset of discrete samples was measured at the  
122 Paleomagnetism Laboratory of the Complutense University of Madrid, Spain (Table S2). A  
123 KLY-4 (Agico) susceptibility bridge was employed, with an applied magnetic field of 300  
124 A/m. Due to the low ferromagnetic content of most samples, each sample was measured ten  
125 times and averaged. The error bars of the magnetic susceptibility data correspond to the  
126 standard deviation of the mean obtained during the averaging procedure.

### 127 **2.2.3 Micropaleontology**

128 Calcareous nannofossil and foraminifera sample preparation and examination followed  
129 standard procedures. Samples for calcareous nannofossils were prepared using standard  
130 smear-slide techniques (Bown and Young, 1998). A small amount of sediment was mixed  
131 with a drop of water on a coverslip, distributed with a toothpick, and then dried on a hot  
132 plate. The coverslip was affixed to a glass microscope slide using Norland Optical Adhesive  
133 61 and cured under an ultraviolet light. Slides were examined on a Leitz Ortholux II POL-BK  
134 microscope under cross-polarized and plane-transmitted light. Nannofossil distribution was  
135 determined for 41 samples extending from Paleocene to the upper lower Eocene (Teurian to  
136 Mangaorapan New Zealand stages) (Table S3). Counts of 400 specimens were conducted at  
137 1000× for each sample, followed by a scan of at least 400 fields of view at 630× to look for  
138 rare taxa). Foraminiferal distribution was determined for 59 samples spanning the same time  
139 interval (Table S4).

140 Foraminiferal biostratigraphy is correlated with New Zealand stages (Cooper, 2004) and  
141 international biozones (Olsson et al., 1999; Pearson et al., 2006). New Zealand stage and  
142 biozone boundaries are calibrated to the 2012 geological timescale (Gradstein et al., 2012)  
143 using criteria described by Raine et al. (2015) and Norris et al. (2014). Foraminiferal  
144 taxonomy is based on Hornibrook et al. (1989), Olsson et al. (1999) and Pearson et al. (2006).  
145 Biostratigraphic results for calcareous nannofossils are correlated to the biostratigraphic  
146 zonation scheme of Martini (1970, 1971), calibrated to the 2012 geological timescale  
147 (Gradstein et al., 2012). Taxonomic concepts for species are those given in Perch-Nielsen  
148 (1985) and Bown (1998).

### 149 **2.2.4 Stable isotopes and carbonate content**

150 Analysis for stable isotopes and carbonate content was undertaken at three laboratories.  
151 Results are tabulated in Table S5. Bulk carbonate  $\delta^{13}\text{C}$  and  $\delta^{18}\text{O}$  measurements were  
152 undertaken at the National Isotope Centre, GNS Science, Lower Hutt. Samples were analysed  
153 on the GVI IsoPrime Carbonate Preparation System at a reaction temperature of 25°C and run  
154 via dual inlet on the IsoPrime mass spectrometer. All results are reported with respect to  
155 VPDB, normalized to the GNS marble internal standard with reported values of 2.04‰ for  
156  $\delta^{13}\text{C}$  and -6.40‰ for  $\delta^{18}\text{O}$ . The external precision ( $1\sigma$ ) for these measurements is 0.05‰ for  
157  $\delta^{13}\text{C}$  and 0.12‰ for  $\delta^{18}\text{O}$ .

158 Individual specimens from five foraminiferal genera were used for stable isotope analysis and  
159 elemental geochemistry. Specimens were selected for analysis based on visual assessment of  
160 their preservation under a stereo microscope. Wherever possible, analyses were performed  
161 on *Morozovella aequa*, *Acarinina coalingensis*, *Subbotina patagonica*, *S. roesnasensis*, and  
162 *Cibicides proprius/praemundulus*, and *Stensioina beccariformis*. The following species were  
163 substituted when these species were not available: *Morozovella subbotinae*, *M. acuta*, *M.*  
164 *apanthesma*, *Acarinina soldadoensis*, *A. subsphaerica*, *A. esnaensis*, *A. nitida* and *Cibicides*  
165 *tholus*. The stable isotope signature of *Acarinina soldadoensis*, *A. subsphaerica*, *A. nitida* and  
166 all species of *Morozovella* indicates they were mixed layer dwellers (Olsson et al., 1999;  
167 Quillévére and Norris, 2003), and therefore are appropriate indicators of near surface  
168 conditions. *Subbotina patagonica* is inferred to have had a deeper planktonic habitat (Pearson  
169 et al., 2006), within the thermocline. There is no data on the habitat of *S. roesnasensis*. Stable  
170 isotope analysis of foraminifera was carried out in the Stable Isotope Laboratory at the  
171 University of California, Santa Cruz. Between 1 and 6 (average of 3) specimens of *Cibicides*,  
172 1 and 5 (average of 3) specimens of *Stensioina*, 3–17 (average of 10) specimens of *Acarinina*,  
173 2–10 (average of 4) specimens of *Morozovella*, and 1–8 (average of 5) specimens of  
174 *Subbotina* were used in each analysis. Specimens were first sonicated in deionised water to  
175 remove clay and detrital calcite. Isotopic measurements were carried out on a Thermo-  
176 Finnigan MAT253 mass spectrometer interfaced with a Kiel Device. The analytical precision  
177 ( $1\sigma$ ) is based on repeat analysis of an in-house standard (Carrara marble), calibrated to the  
178 international standards NBS18 and NBS19, and averages  $\pm 0.05$  ‰ for  $\delta^{13}\text{C}$  and  $\pm 0.08$  ‰ for  
179  $\delta^{18}\text{O}$ . All values are reported relative to VPDB. For the  $\delta^{18}\text{O}$  values of *Cibicides* (= *Cibicidoides*;  
180 see Schweizer et al., 2009) and *Stensioina*, we apply an isotopic correction

181 factor of +0.28 (Katz et al., 2003). Paleotemperatures for both benthic and planktic taxa were  
182 calculated from  $\delta^{18}\text{O}$  using the equation of Kim and O'Neil (1997):

$$183 \quad T (\text{°C}) = 16.1 + -4.64(\delta^{18}\text{O}_M - \delta^{18}\text{O}_{\text{SW}}) + 0.09(\delta^{18}\text{O}_M - \delta^{18}\text{O}_{\text{SW}})^2 \quad (1)$$

184 Where  $\delta^{18}\text{O}_M$  = measured value and  $\delta^{18}\text{O}_{\text{SW}} = -1.23\text{‰}$ , which incorporates a SMOW to PDB  
185 correction of  $-0.27\text{‰}$  (Kim and O'Neil, 1997) and an ice volume component of  $-0.96\text{‰}$   
186 (Zachos et al. , 1994) assuming ice-free conditions for the Paleocene-Eocene transition.  
187 Planktic values are also corrected for paleolatitude (Zachos et al., 1994; correction of  $-0.23\text{‰}$   
188 for  $\sim 65^\circ\text{S}$ ).

189 The carbonate content of dried powdered samples was determined at the National Institute of  
190 Water and Atmosphere (NIWA, Wellington) via gasometric quantitative analysis after  
191 acidification (Jones and Kaiteris, 1983), with a precision of  $\pm 2\%$ . The composition of the  
192 non-carbonate residue was not determined.

### 193 **2.2.5 Elemental geochemistry and Mg/Ca analysis**

194 Foraminifera were picked from the 150–300  $\mu\text{m}$  fraction of washed sediment samples and  
195 individually washed in ultra-pure ( $>18.2 \text{ m}\Omega$ ) water and analytical grade methanol three  
196 times before being mounted on double-sided tape adhered to a glass slide. Mg/Ca analysis  
197 was carried out on 4–19 specimens for each of the selected genera in each sample (Table S6).  
198 Each foraminifer was analysed at least three times using a pulsed ArF laser (Lambda Physik  
199 LPFpro 205) with a 193  $\mu\text{m}$  wavelength, 30  $\mu\text{m}$  spot size, laser power of  $3 \text{ J/cm}^2$  and a  
200 repetition rate of 3 Hz, in conjunction with an ANU HelEx laser ablation cell, at the Research  
201 School of Earth Sciences of the Australian National University. An analysis of the NIST-  
202 SRM610 silicate standard was taken between every 9–12 foraminifer analyses to correct for  
203 elemental fractionation originating from laser ablation and mass-spectrometry effects.

204 The final three chambers of the final whorl in each specimen were analysed individually by  
205 ablating slowly at a rate of  $0.2\text{--}0.3 \mu\text{m s}^{-1}$  to produce a separate trace element profile through  
206 the wall of each chamber (Fig. S1). A Varian 820 LA-ICPMS was used to measure  
207 abundances of the trace metal isotopes  $^{24}\text{Mg}$ ,  $^{27}\text{Al}$ ,  $^{29}\text{Si}$ ,  $^{47}\text{Ti}$ ,  $^{55}\text{Mn}$ ,  $^{66}\text{Zn}$ ,  $^{88}\text{Sr}$  and  $^{138}\text{Ba}$   
208 relative to  $^{43}\text{Ca}$  during ablation. Elemental ratios reported for each sample are average values  
209 derived from multiple screened profile segments for multiple specimens of a given taxon.

210 Laser ablation sites were selected using light microscopy and SEM imaging to avoid zones of  
 211 detrital contamination, recrystallization or test ornamentation that might cause irregular trace  
 212 element/Ca profiles (Fig. S1). Individual chamber profiles were screened to exclude zones  
 213 with anomalously high Mg/Ca, Al/Ca, Mn/Ca or Ba/Ca ratios, which indicate significant  
 214 silicate contamination (Barker et al., 2003; Greaves et al., 2005; Creech et al., 2010). These  
 215 profiles typically show zones of enriched in Mg, Al, Mn, and Ba on the outside and inside  
 216 surfaces of the chamber wall, consistent with silicate contamination (Fig. S1). The Sr/Ca ratio  
 217 is used as an indicator of diagenetic alteration because the concentration of Sr may decrease  
 218 or increase during alteration or secondary calcification (Eggins et al., 2003; Kozdon et al.,  
 219 2013). A ratio of ~1.4 is typical for well-preserved tests (Creech et al., 2010). Therefore,  
 220 samples with Sr/Ca values outside the range of 0.8–1.6 mmol/mol were considered to be  
 221 affected by diagenesis (Fig. 3). Al/Ca and Mg/Ca data show a positive linear correlation  
 222 when plotted (Fig. 3), reflecting the influence of silicate contamination. We have used the  
 223 method of Creech (2010; after Barker et al., 2003) to screen for this contamination. The  
 224 Al/Mg composition of the contaminant phase was identified by plotting Mg/Ca against Al/Ca  
 225 and finding the slope of the linear regression. Once this Al/Mg composition had been  
 226 determined for each genus, the screening threshold was set by calculating the Al/Ca ratio at  
 227 which paleotemperature estimates would be biased by more than 1°C. This screening  
 228 removes anomalously high Mg/Ca values and reduces the mean value for most samples (Fig.  
 229 4, S2). After the measurements have been screened for silicate contamination, the effects of  
 230 diagenesis are more easily assessed (Fig. 3). A weak negative correlation between Sr/Ca and  
 231 Mg/Ca suggests that diagenesis may also cause an increase in Mg/Ca values, especially in the  
 232 planktic genus *Acarinina*. The reasons for this correlation and implications are discussed  
 233 below.

234 Marine paleotemperatures are calculated using the exponential relationship between Mg/Ca  
 235 and temperature (Eq. 2). Because the planktic foraminifera used in this study are extinct, sea  
 236 surface temperatures (SSTs) were calculated using a general calibration based on the mean  
 237 calcification temperatures of nine modern planktic species ( $A = 0.09$ ,  $B = 0.38$ ; Anand et al.,  
 238 2003). Sea floor temperatures (SFTs) were calculated using the calibration of Lear et al.  
 239 (2002) based on three benthic species of *Cibicoides/Cibicides* ( $A = 0.109$ ,  $B = 0.867$ ):

$$240 \quad Mg/Ca_{test} = \left( \frac{Mg/Ca_{sw}^{t=t}}{Mg/Ca_{sw}^{t=1}} \right) \times B \exp^{AT} \quad (2)$$



241 Marine temperature reconstructions based on early Eocene foraminiferal calcite have shown  
 242 that a high (>3 mol/mol) Mg/Ca<sub>sw</sub> value is required to reconcile Mg/Ca-derived  
 243 paleotemperatures with those derived from δ<sup>18</sup>O (Lear et al., 2002; Sexton et al., 2006). High  
 244 Mg/Ca<sub>sw</sub> values are in line with modelled values from Wilkinson & Algeo (1989) but are at  
 245 odds with several proxy studies (e.g., Horita et al., 2004; Coggon et al., 2010) and more  
 246 recent modelling (e.g., Stanley & Hardie, 1998) that favour lower values for Mg/Ca<sub>sw</sub> (<2  
 247 mol/mol). However, recent studies (Hasuik & Lohmann, 2010, Evans & Müller, 2012) have  
 248 reconciled the empirical relationship between δ<sup>18</sup>O and Mg/Ca paleotemperatures with these  
 249 lower values for Mg/Ca<sub>sw</sub> by showing that a power law distribution, rather than an  
 250 exponential distribution, better describes the relationship between Mg-partitioning and  
 251 temperature in foraminiferal calcite:

$$252 \quad Mg/Ca_{test} = \left( \frac{B}{Mg/Ca_{sw}^{t=0H}} \right) \times Mg/Ca_{sw}^{t=tH} \exp^{AT} \quad (3)$$

253 To apply this equation we use exponential and pre-exponential calibration constants from  
 254 modern multispecies calibrations and paleotemperature values derived from oxygen isotopes  
 255 to estimate the function *H* for extinct foraminifera. Published data from well-preserved  
 256 Eocene foraminifera at Hampden Beach (Burgess et al., 2008; Hollis et al., 2012) and  
 257 Tanzania (Pearson et al., 2007), for which paired Mg/Ca and δ<sup>18</sup>O data is available, have been  
 258 used to derive *H* for the extinct species used in this study.

259 In calculating the value of *H*, we have used an early Eocene Mg/Ca<sub>sw</sub> value of 1.6 mol/mol  
 260 (Stanley & Hardie, 1998; Evans & Müller, 2012) and a modern Mg/Ca<sub>sw</sub> value of 5.17  
 261 mol/mol. This *H* value does not take into account possible variability in Mg/Ca<sub>sw</sub> values  
 262 through the early Paleogene. The Mg/Ca-temperature calibrations of Anand et al. (2003) and  
 263 Lear et al. (2002) have been used, although it is likely that the pre-exponential constant of  
 264 Paleogene planktic foraminifera differed from that of the modern taxa. We calculate an *H*  
 265 value of 20 for Paleogene planktic foraminifera, which is significantly lower than *H* values  
 266 for modern planktics, such as *Globigerina sacculifer* (*H* = 0.42; Hasuik & Lohmann, 2010).  
 267 For benthic foraminifera, Cramer et al. (2011) suggest that the value of *H* would be similar  
 268 between *Cibicides* sp. and *Oridorsalis umbonatus*. The calculation for Mg/Ca-derived  
 269 temperature values is.

$$T = \frac{\ln\left(\frac{[Mg/Ca_{test}] \times [Mg/Ca_{SW}^{t=0}]^H}{B \times [Mg/Ca_{SW}^{t=t}]^H}\right)}{A} \quad (4)$$

271 Temperature values derived from Mg/Ca ratios of surface mixed-layer dwelling taxa used in  
 272 this study are normalised to *Morozovella crater* following Creech et al. (2010). Three types  
 273 of error are applied to paleotemperatures derived from Mg/Ca ratios; the analytical error,  
 274 sample error and a standard calibration error. The analytical error is accounted for in the data  
 275 processing step, and typically produces very small uncertainties ( $\pm 1\text{--}3\%$  2se) associated with  
 276 counting statistics during ablation and data acquisition. The sample error pertains to the 95%  
 277 confidence interval calculated for the mean temperature value obtained from multiple  
 278 analyses within a single sample, and is calculated by:

$$\bar{X} \pm t \times \frac{\sigma}{\sqrt{n}} \quad (5)$$

280 Where  $\bar{X}$  is the sample mean,  $t$  is the inverse of the Students' t-distribution,  $\sigma$  represents the  
 281 standard deviation and  $n$  is the number of analyses. The calibration error is the residual error  
 282 of  $\pm 1.6^\circ\text{C}$  on the regression of the multispecies calibrations established by Lear et al. (2002)  
 283 and Anand et al. (2003). The cumulative error calculated from the sum of all three errors is  
 284 applied to each temperature value, providing upper and lower uncertainties.

### 285 **3 Results and Discussion**

#### 286 **3.1 Stratigraphy**

287 The 45 m-thick studied interval (425–470 mbsf) consists of five cores, with significant gaps  
 288 due to poor recovery in three of the cores, which extend from middle Paleocene to lower  
 289 Eocene (Fig. 2). The sediments are greenish-white to greenish-grey nannofossil chalk, with  
 290 higher clay content in the upper Paleocene (core 46; 463–470 mbsf) and lowermost Eocene  
 291 (core section 45-3; 456.96–457.3 mbsf)) and minor glauconite (cores 43-44) and chert  
 292 nodules (cores 41-43) in the overlying Eocene. A record of “incipient chert” in core section  
 293 45–3 (Kennett et al., 1975) may have been a misidentification of the darker-grey clay-rich  
 294 sediments at the base of the PETM (Fig. 5).

295 Calcareous microfossils are only moderately preserved overall, and there is an interval  
 296 directly below the Paleocene-Eocene boundary (457.3 to 457.58 mbsf) in which foraminifera

297 are poorly preserved and sparse. Planktic foraminifera are used to correlate the 45 m-thick  
298 studied interval to New Zealand stages (Teurian to Mangaorapan) and to international  
299 foraminiferal zones P4a-b to E7 (Fig. 2). Nannofossil assemblages over the same interval  
300 have been correlated with nannofossil zones NP6 to NP12. Whereas previous studies  
301 indicated an undifferentiated upper Paleocene succession spanning Zone NP6–8 (Edwards  
302 and Perch-Nielsen, 1975; Hollis et al., 1997), we infer a ~2 Myr hiatus near the top of Core  
303 46 (463.49–463.16 mbsf), representing all of zones NP7 and NP8. Immediately above the  
304 hiatus, *Discoaster multiradiatus* makes up ~2% of the assemblage, suggesting that the  
305 lowermost part of Zone NP9 is missing. This lowest occurrence (LO) of *D. multiradiatus*  
306 coincides with the LOs of *D. lenticularis* and *D. salisburgensis*.

307 The PETM is a 34 cm-thick interval within core 45 (457.3–456.96 mbsf) that is clearly  
308 delineated by a 40% decrease in carbonate content and 2–3‰ negative excursions in bulk  
309 carbonate  $\delta^{13}\text{C}$  and  $\delta^{18}\text{O}$  values (Fig. 2). The Benthic Foraminiferal Extinction Event (BFEE)  
310 is identified directly below the PETM at 457.3 mbsf based on the highest occurrences of the  
311 *Stensioina beccariformis*, *Gyroidinoides globosus* and *G. subangulatus*. The planktic  
312 foraminiferal genus *Morozovella* has its lowest occurrence at the base of the PETM and  
313 greatest diversity within the PETM. *Morozovella aequa* and *M. velascoensis* are restricted to  
314 the PETM. The latter species has rarely been found outside the PETM in the SW Pacific but  
315 *M. aequa* ranges into the middle late Eocene in New Zealand sections (Hornibrook et al.  
316 1989). For nannofossils, taxa typical of the PETM in other regions, such as the *Rhomboaster*  
317 lineage, *Discoaster araneus* and *D. anartios* (e.g., Bybell and Self-Trail, 1994; Kahn and  
318 Aubry, 2004), are absent here. Instead, the nannofossil assemblage is characterized by  
319 deformed *Discoaster* specimens, many similar to *Discoaster nobilis* (e.g., Raffi and De  
320 Bernardi, 2008), as well as increased abundance of *Coccolithus* spp. and the presence of  
321 *Fasciculithus* spp. and *Bomolithus supremus*, which is restricted to the PETM interval at this  
322 site. Immediately above the PETM (456.92 mbsf), the abundances of *Fasciculithus* spp. and  
323 *Coccolithus* spp. decrease significantly, with a concomitant increase in *Zygrhablithus*  
324 *bijugatus*. As discussed below, the stable isotope record through the P-E transition indicates  
325 that the PETM is truncated, with only the onset and body of the CIE represented by these 34  
326 cm of sediment.

327 An age-depth plot (Fig. S3) based on calcareous nannofossil and foraminiferal bioevents  
328 (Table S7) provides a preliminary guide to compacted sedimentation rates. This rate appears  
329 to have been relatively low in the Paleocene (0.4 to 0.45 cm/kyr) either side of the hiatus at  
330 ~463.4 mbsf, but approximately four times higher in the early Eocene (1.68 cm/kyr).  
331 However, a rather patchy distribution of events and uncertainty over the duration of hiatuses  
332 means that it is possible to construct an alternative age model in which rates were consistent  
333 across the Paleocene-Eocene transition (dashed line in Fig. S3). Although this implies that the  
334 sedimentation rate for the PETM interval could lie anywhere between the low Paleocene rate  
335 and the high Eocene rate, the lower rate is consistent with the duration of the CIE from onset  
336 to  $\delta^{13}\text{C}$  minimum, i.e., ~45-66 kyrs (Röhl et al., 2007).

337 The base of the PETM coincides with a distinct colour change to a darker greenish-grey chalk  
338 that grades back into greenish-white chalk over 15 cm (Fig. 5). This dark interval is also  
339 highly burrowed. Burrowing is also evident in other parts of the core but it is less obvious in  
340 more pale lithologies. XRF core scanning shows an increase in Fe content at the base of this  
341 interval, followed by a cyclical decrease to background levels at 456.95 m (Fig. 5A). A lower  
342 resolution record of magnetic susceptibility in discrete samples reveals a similar trend: a peak  
343 near the base of the darker interval, followed by a quasi-cyclical decrease to background  
344 levels. The peaks are inferred to represent intervals of higher clay content based on the  
345 parallel trends in Fe and magnetic susceptibility. Many of the other peaks and troughs in the  
346 Fe record below and above the PETM are scanning artefacts related to core breaks. However,  
347 parallel peaks in magnetic susceptibility and Fe content in the lower part of core 45 (~457.7  
348 mbsf) appears to be a robust signal although the cause is unknown. There are no  
349 accompanying changes in isotopic signature or obvious lithological changes at this level.

350 A 10 cm interval directly below the PETM also has a reduced carbonate concentration but  
351 there is no change in  $\delta^{13}\text{C}$  (Fig. 2, 5B). As there is no accompanying increase in magnetic  
352 susceptibility or Fe content (Fig. 5A), the decrease in carbonate content seems to be due to an  
353 increase in silica, perhaps associated with the slight cooling indicated by a small positive shift  
354 in  $\delta^{18}\text{O}$  of ~0.4‰ in both bulk and foraminiferal calcite (Fig. 2, 5D). Although the silica is  
355 presumed to be biogenic, siliceous microfossils have not been recovered from this interval.

356 For a sedimentation rate of 0.45 cm/kyr, the 34 cm thick PETM interval represents ~76 kyrs  
357 and the three peaks in Fe content represent a periodicity close to the precession band (~21

358 kyrs). Indeed, there is good agreement between the Fe cycles and  $\delta^{13}\text{C}$  record at Site 277 and  
359 ODP Site 690 (Röhl et al., 2007), where the negative CIE occurs over three steps and the  
360  $\delta^{13}\text{C}$  minimum (Horizon C of Zachos et al., 2005) occurs within the third Fe peak. Based on  
361 this correlation with Site 690, we infer that the interval from the CIE onset to the base of  
362 Cycle 4 is preserved at Site 277, or the first 66 kyrs of the PETM (Röhl et al., 2007),  
363 implying a slight increase in sedimentation rate through the PETM (52 cm/kyr).

### 364 **3.2 Stable isotopes**

365 Bulk carbonate stable isotopes display a significant offset between  $\delta^{18}\text{O}$  and  $\delta^{13}\text{C}$  minima,  
366 with the  $\delta^{18}\text{O}$  minimum occurring at the base and the  $\delta^{13}\text{C}$  minimum in the upper part of the  
367 PETM (Fig. 2, 5B). The negative CIE of  $\sim 2\text{‰}$  is slightly smaller than the average for marine  
368 sections ( $2.7\text{‰}$ ; McInerney and Wing, 2011) and occurs gradually over the lower 20 cm of  
369 the PETM. In contrast, the  $3\text{‰}$  negative  $\delta^{18}\text{O}$  excursion (OIE) is abrupt at the base of the  
370 PETM and is larger in magnitude than is known elsewhere (e.g., Bains et al. 1999; Dunkley  
371 Jones et al., 2013). If this is a primary feature and due solely to a change in temperature, this  
372 excursion would equate to  $\sim 12^\circ\text{C}$  of warming (Fig. 5D); however, the OIE is most likely  
373 accentuated by diagenesis as is discussed below.

374 Examination of foraminiferal  $\delta^{18}\text{O}$  and Mg/Ca ratios help to separate the diagenetic effects  
375 from the paleotemperature record. As none of the foraminifera recovered in this study have  
376 “glassy” preservation (Sexton et al. 2006; Pearson and Burgess, 2008; Kozdon et al., 2013),  
377 all are assumed to have been altered to varying degrees. We selected the best preserved  
378 specimens for isotopic analysis (Fig. 2, 5B, 6). Our results indicate that normal surface to  
379 deep  $\delta^{13}\text{C}$  gradients are preserved in the foraminiferal tests, with bulk carbonate  $\delta^{13}\text{C}$  values  
380 lying within the range of, or slightly lighter than, planktic foraminiferal  $\delta^{13}\text{C}$  throughout the  
381 studied interval. An exception is noted in the basal PETM where two values are more positive  
382 than planktic  $\delta^{13}\text{C}$  (Fig. 5B, 6B). Benthic  $\delta^{13}\text{C}$  values are  $>0.7\text{‰}$  lighter than both planktic  
383 and bulk carbonate values, apart from the basal PETM sample where a negative gradient of -  
384  $0.37\text{‰}$  occurs between *Acarinina* and *Cibicides* (Fig. 5B, 6B). The implication is that the  
385 onset of the CIE is recorded more strongly in planktic foraminifera (i.e. surface water CIE of  
386  $-1.85\text{‰}$ ) than in either benthic foraminifera (deep water CIE of  $-0.55\text{‰}$ ) or bulk carbonate  
387 (CIE of  $-0.34\text{‰}$  across equivalent sample interval).

388 If it were not for the large magnitude of the OIE across the same sample interval (-1.42‰,  
389 and -2.82‰ for the full OIE), we might argue for mixing across the boundary dampening the  
390 bulk carbonate CIE. However, the marked differences in the pattern of onset for the CIE and  
391 OIE suggest that there was no mixing of sediment across the boundary. Similarly, there is  
392 little evidence for the isotope record being affected by carbonate dissolution or burn-down  
393 (Dickens, 2000; Kozdon et al, 2013) below the base of the PETM. A weak positive shift in  
394 pre-PETM  $\delta^{18}\text{O}$  values and reduced carbonate content appears to reflect cooler conditions as  
395 the shift is accompanied by a cooling trend in the benthic Mg/Ca ratio (Fig. 5D-E).

396 A similar offset between bulk and planktic  $\delta^{13}\text{C}$  in the basal PETM was described for ODP  
397 Site 690, where Stoll (2005) showed close agreement between trends in stable isotopes for  
398 bulk carbonate, coccolith fractions and *Subbotina* but significant offsets with *Acarinina*, the  
399 latter recording an earlier CIE onset and a later OIE minimum. Stoll (2005) considered  
400 several possible causes for this offset and favoured differences in habitat and seasonal  
401 production. For Site 690, the correspondence between coccoliths and *Subbotina* suggests that  
402 coccolith production may have occurred at a lower level within the photic zone than the level  
403 preferred by *Acarinina*. For Site 277, the  $\delta^{13}\text{C}$  gradient suggests a similar explanation but a  
404 different relationship. During the PETM onset, coccolith production appears to have occurred  
405 at a shallower level than that preferred by planktic foraminifera at this site. This may also  
406 explain why bulk carbonate  $\delta^{18}\text{O}$  is more depleted than planktic values in this interval, i.e.  
407 coccolith production in shallower and warmer waters. Given that this relationship is only  
408 fully expressed at the PETM onset, we suggest that this might have been a time of increased  
409 stratification and differentiation between water masses in the upper water column at this site.  
410 Nunes and Norris (2006) used ageing gradients in benthic  $\delta^{13}\text{C}$  to infer a switch in deep water  
411 formation across the P/E boundary from the Southern Ocean to the Northern Hemisphere.  
412 Our benthic  $\delta^{13}\text{C}$  data from Site 277 support this hypothesis. Site 277 benthic  $\delta^{13}\text{C}$  is 0.46‰  
413 higher than values in the equatorial Pacific prior to the PETM but 0.12‰ lower within the  
414 PETM. It seems likely that comparable changes occurred in surface water circulation.

415 With the CIE onset seeming explicable in terms of relationships between coccolith and  
416 foraminiferal niches and changes in ocean circulation, we turn our attention to the stepped  
417 decline in the bulk carbonate CIE at Site 277. Stoll (2005) argued that a similar series of  
418 three steps in the bulk carbonate CIE seen at Site 690 reflect the greater capacity for

419 coccoliths to record changes in ocean conditions at a finer scale than is possible from the less  
420 abundant foraminiferal fraction. Although we lack the resolution in the foraminiferal record  
421 to compare sites 277 and 690 in detail, we observe the same trend and note a broad  
422 correlation with the three Fe peaks. It seems likely that these steps represent precessional  
423 modulation of the release of  $^{13}\text{C}$ -depleted carbon into the ocean over  $\sim 60$  kyrs (Röhl et al.,  
424 2007; Sluijs et al., 2007).

### 425 **3.3 Diagenetic modification of $\delta^{18}\text{O}$ values**

426 As noted above, bulk carbonate  $\delta^{18}\text{O}$  values at Site 277 intergrade between benthic and  
427 planktic foraminiferal values in the Paleocene and in the Eocene interval above the PETM  
428 (Fig. 6A, 6C). Moreover, several planktic foraminiferal  $\delta^{18}\text{O}$  values are only  $\sim 0.3\%$  lighter  
429 than benthic values in the Paleocene (Fig. 2, 6C). Conversely, all bulk carbonate  $\delta^{18}\text{O}$  values  
430 lie within the range of planktic foraminiferal  $\delta^{18}\text{O}$  within the PETM (Fig. 6B) and, indeed,  
431 bulk carbonate  $\delta^{18}\text{O}$  is lighter than planktic foraminiferal  $\delta^{18}\text{O}$  in the basal PETM (Fig. 2,  
432 5D). We contend that diagenetic effects explain these relationships. The bulk carbonate  $\delta^{18}\text{O}$   
433 has been shifted toward heavier values during early diagenesis (at seafloor temperature) over  
434 much of the section above and below the CIE (Schrag et al., 1995; Sexton et al., 1996;  
435 Kozdon et al, 2013), whereas within the PETM interval the bulk and foraminiferal carbonate  
436 appears to have undergone less diagenetic alteration. We suggest that the increase in clay in  
437 the PETM protected coccoliths and foraminifera from wholesale recrystallization, preserving  
438 more of the original  $\delta^{18}\text{O}$  signal. The presence of clay serves to reduce sediment porosity and  
439 retard carbonate recrystallization (Sexton et al., 2006). This explains the large magnitude of  
440 the bulk carbonate  $\delta^{18}\text{O}$  excursion across the P-E boundary, with the  $\delta^{18}\text{O}$  values below the  
441 excursion having been altered toward heavier values (Fig. 2, 5D-E).

442 The planktic foraminiferal  $\delta^{18}\text{O}$  values at Site 277 appear to be compromised to varying  
443 degrees by seafloor diagenesis throughout the interval studied. The surface-to-deep  
444 temperature gradient may be expected to be reduced in high latitude regions such as the  
445 Campbell Plateau. Mean annual Subantarctic Water is  $\sim 6^\circ$  warmer than Antarctic  
446 Intermediate Water in the present-day Southern Ocean (Carter et al., 1999). However, the  
447 very low planktic-benthic  $\delta^{18}\text{O}$  gradient in the Paleocene and post-PETM Eocene ( $0.8\%$ ,  
448  $3^\circ\text{C}$ ) suggests alteration of planktic  $\delta^{18}\text{O}$  toward benthic values (Fig. 2, 5D, 6C). The gradient  
449 is only slightly higher in the PETM ( $1.1\%$ ,  $4^\circ\text{C}$ ), suggesting that a cool bias affects all

450 paleotemperatures derived from planktic  $\delta^{18}\text{O}$  through the P-E transition at this site. The  
451 degree of this bias is uncertain. The warmer paleotemperature derived from Mg/Ca ratios  
452 may be more reliable but, as is discussed below, diagenesis may result in a warm bias.

### 453 **3.4 Diagenetic modification of Mg/Ca ratios**

454 There is evidence that diagenesis also has significant and specific effects on Mg/Ca values  
455 (Oomori et al., 1987; Kozdon et al., 2013). As noted earlier, we observe a distinct  
456 relationship between the Mg/Ca ratio and the geochemical proxy for diagenesis, the Sr/Ca  
457 ratio, once we have screened for silicate contamination (Fig. 3). For *Cibicides*, the full  
458 screened dataset shows a roughly horizontal trend, with little change in Sr/Ca as Mg/Ca  
459 varies. This suggests that this genus is relatively immune to the effects of diagenesis, perhaps  
460 related to its relatively thick and smooth wall. However, if we consider Paleocene and PETM  
461 samples separately, we observe that Paleocene analyses tend to have lower Sr/Ca ratios than  
462 PETM samples and exhibit a weak trend in which Mg/Ca increases as Sr/Ca decreases. This  
463 general relationship has also been identified by Kozdon et al. (2013) as a guide to diagenetic  
464 alteration, albeit the impact on Mg/Ca ratios is an order of magnitude smaller than found in  
465 laboratory experiments (Oomori et al., 1987). The trend is more obvious in *Acarinina* at Site  
466 277, probably because the thinner-walled and more irregular test provides more surfaces for  
467 interaction with pore waters and hence facilitates diagenetic alteration. For the full data set, a  
468 significant negative correlation is observed, with Mg/Ca increasing as Sr/Ca decreases. A  
469 weaker trend is evident in the PETM data but a much stronger trend is shown by the  
470 Paleocene data. From these observations we can draw the following conclusions: (i)  
471 *Acarinina* is more prone to diagenesis than *Cibicides*, (ii) diagenesis is greater in the  
472 Paleocene than in the PETM, and (iii) diagenesis causes an increase in the Mg/Ca ratio and  
473 implies that paleotemperatures may be overestimated for some taxa, such as *Acarinina*, and  
474 in some intervals such as the Paleocene at this site. This may explain why the SST estimates  
475 for the Paleocene based on *Acarinina* Mg/Ca ratios are higher than expected (Fig. 5D, E).

### 476 **3.5 Paleotemperature**

477 Taking into account these numerous complications, we can make some general observations  
478 on temperature changes through the P-E transition at Site 277. Estimates for SFT from  
479 benthic foraminiferal  $\delta^{18}\text{O}$  and Mg/Ca are relatively consistent at 12–15°C for the late



480 Paleocene (Fig. 5D), with coolest SFTs of 11–12°C occurring in the uppermost 10 cm of  
481 Paleocene where carbonate content is also lower than background. Benthic  $\delta^{18}\text{O}$  and Mg/Ca  
482 values indicate SFT warmed by ~5–6°C across the P-E boundary, with SFTs of up to ~19°C  
483 in the basal PETM. There is little evidence for further warming of SFT in the body of the  
484 PETM. Following the PETM, SFT drops abruptly by ~5°C and remains stable at ~13°C in the  
485 overlying Eocene interval (Fig. 5D–E). Diagenesis may explain why some Paleocene Mg/Ca  
486 ratios yield higher SFTs than the benthic  $\delta^{18}\text{O}$  values.

487 The SST record across the P-E boundary is much more difficult to interpret. The small offset  
488 between benthic and planktic  $\delta^{18}\text{O}$  (~3°C) combined with the large offset between planktic  
489  $\delta^{18}\text{O}$  and Mg/Ca values (~12°C) in the Paleocene, are likely consequences of diagenetic  
490 alteration, with the actual SST lying somewhere between 15 and 27°C (Fig. 5D). Similarly,  
491 the degree of warming across the PETM may be accentuated for  $\delta^{18}\text{O}$  but effectively  
492 dampened for Mg/Ca due to the effects discussed above. For this reason, the observation that  
493 the relative SST increase is ~5–6°C for both proxies (Fig. 5E) is difficult to explain even  
494 though it is consistent with the SFT record. Diagenetic effects appear to decrease across the  
495 P-E boundary, based on our analysis of the benthic–planktic  $\delta^{18}\text{O}$  gradient and the Sr/Ca  
496 ratio. Therefore, we would predict that the relative increase in SST across the boundary  
497 would be greater for planktic  $\delta^{18}\text{O}$  than for Mg/Ca. It may be that the patchy nature of the  
498 record through this interval is masking these relationships. Irrespective of the true magnitude  
499 of SST change across the P-E boundary, planktic Mg/Ca ratios indicate warmest SSTs in the  
500 lower PETM, stable SSTs through the body of the PETM (albeit ~3°C cooler) and an abrupt  
501 ~4°C cooling directly above the PETM.

502 The 5–6°C increase in SST is similar to other PETM records. At ODP Site 1172, the  $\text{TEX}_{86}$   
503 record indicates that SST increased by 6°C across the P-E boundary (Sluijs et al., 2011) and  
504 SST during the PETM was 3–4°C warmer than average Paleocene values (Fig. 7). Elsewhere,  
505 temperature anomalies within the PETM range from +4–5°C in low latitudes (Zachos et al.,  
506 2003; Aze et al., 2014) to +8°C in high latitudes (Thomas et al., 2002; Frieling et al., 2014)  
507 and some low latitude coastal sites (Zachos et al., 2006).

508 The peak SSTs of ~32°C within the PETM are consistent with  $\text{TEX}_{86}$ -based SSTs from the  
509 PETM at ODP Site 1172 (Sluijs et al., 2011) and in the mid-Waipara section, eastern South  
510 Island, New Zealand (Hollis et al., 2012). At these locations, the two calibrations for  $\text{TEX}_{86}$

511 introduced by Kim et al. (2010) yield peak SSTs for the PETM of 32–34°C (TEX<sub>86</sub><sup>H</sup>) or 26–  
512 28°C (TEX<sub>86</sub><sup>L</sup>). Although the TEX<sub>86</sub><sup>L</sup> calibration was considered more suitable for this region  
513 based on comparisons with other SST proxies (Hollis et al., 2012), a new Bayesian approach  
514 to TEX<sub>86</sub> calibrations (Tierney and Tingley, 2014) yields temperatures for the PETM that are  
515 very similar to the TEX<sub>86</sub><sup>H</sup> calibration. These PETM SSTs are also consistent with the SST  
516 estimates of 26°C that were derived from TEX<sub>86</sub> and U<sup>K</sup><sub>37</sub> for the late Eocene at Site 277  
517 (Liu et al, 2009), given that deep sea temperatures cooled by ~8°C through the Eocene  
518 (Zachos et al., 2008).

519 There is considerable debate about the veracity of such high temperature estimates in high  
520 latitude regions, with concerns raised about calibrations, seasonal bias and archaeol  
521 physiology processes (Sluijs et al., 2006; Hollis et al., 2012; Taylor et al. 2013; Inglis et al.,  
522 2015). However, the consistency between SSTs derived from Mg/Ca and TEX<sub>86</sub> (Burgess et  
523 al., 2008; Hollis et al., 2012) suggests that the high temperatures are due to factors that the  
524 proxies may have in common, such as a warm-season bias, rather than problems with  
525 respective calibrations or physiological factors.

### 526 **3.6 Comparison with other PETM records**

527 A comparison of the PETM record at DSDP Site 277 with nearby records at Mead Stream  
528 (Hollis et al., 2005a; Nicolo et al., 2010) and ODP Site 1172 (Sluijs et al., 2011) reveals  
529 several significant features (Fig. 7). Firstly, there seems little doubt that only the onset of the  
530 CIE is preserved at Site 277. The pattern of decreasing  $\delta^{13}\text{C}$  is very similar to the expanded  
531 onset at Mead Stream. As noted above, the stepped decrease in  $\delta^{13}\text{C}$  is also observed at ODP  
532 Site 690 (Röhl et al., 2007). However, the pattern of warming at Site 277 is different from  
533 Site 1172. At Site 277, the most pronounced increase in temperatures occurs at the base of the  
534 PETM and is associated with a weak negative  $\delta^{13}\text{C}$  excursion. Higher in the PETM,  
535 temperatures remain stable or decrease slightly as  $\delta^{13}\text{C}$  decreases. At Site 1172, the TEX<sub>86</sub>  
536 record indicates pronounced warming at the base of the PETM but SST continues to increase  
537 and peaks just above the  $\delta^{13}\text{C}$  minimum. No direct measurements of temperature have been  
538 obtained from the indurated lithologies at Mead Stream. However, changes in radiolarian  
539 assemblages identify a definite peak in low-latitude species, also directly above the  $\delta^{13}\text{C}$   
540 minimum (red star in Fig. 7) (Hollis, 2006).

541 The implication of these differences between SW Pacific sites is that the primary warming  
542 pulse occurred in both intermediate and surface waters at the initiation of the PETM on the  
543 Campbell Plateau, whereas this initial event was only the precursor to progressive warming in  
544 the continental margin settings to the west and north (Fig. 1). A similar pattern of warming is  
545 evident in the Atlantic Ocean, where the  $\delta^{18}\text{O}$  records for ODP sites 690 and 1051 suggest  
546 that peak warming occurred at the onset of the PETM in the southern Atlantic (Site 690) but  
547 at the same level as the CIE minimum in the western North Atlantic (Bains et al., 1999; Stoll,  
548 2005). We cannot be sure that there was not a second warming pulse above the onset of the  
549 PETM on the Campbell Plateau because the main phase of the PETM does not appear to be  
550 preserved at Site 277. However, the absolute SST values at Site 277 are similar to the peak  
551 SSTs at Site 1172, i.e. 30–32°C. Therefore, we need to explain how the Campbell Plateau  
552 warmed at the start of the PETM and stayed warm through the onset, while the East Tasman  
553 Plateau warmed to a lesser extent initially but then continued to warm into the main phase of  
554 the PETM, with both sites experiencing at least seasonal SST maxima in excess of 30°C. We  
555 speculate that the gradual warming that followed Southern Ocean cooling at 59 Ma (Hollis et  
556 al., 2014) exceeded a threshold at the start of the PETM that caused the southward expansion  
557 of the subtropical-tropical gyre over the Campbell Plateau. This gyre was sustained through  
558 the PETM onset but resulted in no additional warming at this location. It is notable that  
559 several warm-water species of *Morozovella* are restricted to the PETM at Site 277. The  
560 influence of the gyre may have also reached the East Tasman Plateau but an additional factor  
561 continued to warm the region into the main phase of the PETM. This factor may have been a  
562 proto-Eastern Australian Current, intensifying its southwestern reach during times of extreme  
563 warming (e.g. Cortese et al., 2013).

#### 564 **4 Conclusions**

565 Part of the motivation in undertaking this study and presenting these results is that there is  
566 interest in re-drilling this site as part of IODP Proposal 567 (Paleogene South Pacific APC  
567 Transect) using new technology that will greatly improve the quantity and quality of core  
568 recovery. We have shown that even with this improved recovery, extracting a paleoclimate  
569 record will still be complicated by diagenesis, recrystallization and hiatuses. In order to  
570 recover a more reliable climate proxy records for the Paleogene of this region, we  
571 recommend consideration of alternative or additional Campbell Plateau sites where

572 sedimentation rates and clay input is predicted to have been higher than at Site 277 (Cook et  
573 al., 1999). Nevertheless, we have also illustrated how a multi-proxy approach can be used to  
574 extract a climate history from this complicated record with due consideration of the effects of  
575 differential diagenesis, both between taxonomic groups and across stratigraphic horizons.

576 The onset of the PETM is recorded in a 34 cm thick interval within core 45 at DSDP Site  
577 277. A significant and rapid warming of surface and deep waters at the onset of the PETM at  
578 Site 277 parallels a pronounced decline in carbonate concentration and a modest initial  
579 negative  $\delta^{13}\text{C}$  excursion of  $\sim 1\text{‰}$ . The full extent of the  $2\text{‰}$  negative  $\delta^{13}\text{C}$  excursion occurred  
580 gradually over an interval in which temperatures remained stable or declined slightly.  
581 Therefore, it would seem that an initial carbon perturbation had a pronounced effect on  
582 southern Pacific Ocean circulation, causing poleward expansion of warm surface and  
583 intermediate waters. In contrast, the full expression of the event had little additional effect,  
584 perhaps because a threshold was exceeded at the initial event.

#### 585 **Acknowledgements**

586 This research relied on archival DSDP samples and data provided by the International Ocean  
587 Discovery Program (IODP) and was funded by the New Zealand Government through the  
588 GNS Science Global Change through Time Programme (540GCT12, 540GCT62). We thank  
589 Paul Pearson and Reinhard Kozdon for very constructive reviews, Appy Sluijs for editorial  
590 handling, and Randall McDonnell (GNS Science) for technical support.

591

592

#### 593 **References**

594 Anand, P., Elderfield, H., and Conte, M. H: Calibration of Mg/Ca thermometry in planktonic  
595 foraminifera from a sediment trap time series, *Paleoceanography* 18 (2), 1050, doi:  
596 10.1029/2002pa000846, 2003.

597 Aubry, M. -P., Ouda, K., Dupuis, C., Berggren, W. A. and Van Couvering, J. A.: The Global  
598 Standard Stratotype-section and Point (GSSP) for the base of the Eocene Series in the  
599 Dababiya section (Egypt), *Episodes* 30, 271-286, 2007.

600 Aze, T., Pearson, P. N., Dickson, A. J., Badger, M. P. S., Bown, P. R., Pancost, R. D., Gibbs,  
601 S. J., Huber, B. T., Leng, M. J., Coe, A. L., Cohen, A. S. and Foster, G. L.: Extreme warming  
602 of tropical waters during the Paleocene–Eocene Thermal Maximum, *Geology* 42, 739-742,  
603 2014.

604 Bains, S., Corfield, R. M. and Norris, R. D.: Mechanisms of climate warming at the end of  
605 the Paleocene, *Science* 285, 724-727, 1999.

606 Barker, S., Greaves, M. and Elderfield, H.: A study of cleaning procedures used for  
607 foraminiferal Mg/Ca paleothermometry, *Geochemistry, Geophysics, Geosystems* 4, 8407,  
608 doi:8410.1016/j.quascirev.2004.8407.8016, 2003.

609 Beerling, D. J., Royer, D. L.: Convergent Cenozoic CO<sub>2</sub> history, *Nature Geoscience* 4, 418-  
610 420, 2011.

611 Bown, P. R. (Ed.): *Calcareous Nannofossil Biostratigraphy*, Kluwer Academic, London,  
612 315p., 1998.

613 Bown, P. R., Young, J. R.: Techniques. In: Bown, P. R. (Ed.), *Calcareous Nannofossil*  
614 *Biostratigraphy*, Kluwer Academic, London, 16–28, 1998.

615 Burgess, C. E., Pearson, P. N., Lear, C. H., Morgans, H. E. G., Handley, L., Pancost, R. D.,  
616 Schouten, S.: Middle Eocene climate cyclicity in the southern Pacific: Implications for global  
617 ice volume, *Geology* 36, 651-654, 2008.

618 Bybell, L. M. and Self-Trail, J. M.: Evolutionary, biostratigraphic, and taxonomic study of  
619 calcareous nannofossils from a continuous Paleocene-Eocene boundary section in New  
620 Jersey, US Geological Survey Professional Paper 1554, 114 p, 1994.

621 Carter, R. M., McCave, I. N. and Richter, C. et al.: Proceedings of the Ocean Drilling  
622 Program, initial reports, volume 181: Southwest Pacific gateways, Sites 1119-1125, 1999.

623 Coggon, R. M., Teagle, D. A. H., Smith-Duque, C. E., Alt, J. C. and Cooper, M. J.:  
624 Reconstructing Past Seawater Mg/Ca and Sr/Ca from Mid-Ocean Ridge Flank Calcium  
625 Carbonate Veins, *Science* 327, 1114-1117, 2010.

626 Cook, R. A., Sutherland, R. and Zhu, H.: Cretaceous–Cenozoic geology and petroleum  
627 systems of the Great South Basin, New Zealand, Institute of Geological & Nuclear Sciences  
628 Monograph 20, 190 pp., 1999.

629 Cooper, R. A. (Ed.): The New Zealand Geological Timescale, Institute of Geological and  
630 Nuclear Sciences Monograph 22, 284 pp., 2004.

631 Cortese, G., Dunbar, G. B., Carter, L., Scott, G., Bostock, H., Bowen, M., Crundwell, M.,  
632 Hayward, B. W., Howard, W., Martinez, J. I., Moy, A., Neil, H., Sabaa, A. and Sturm, A.:  
633 Southwest Pacific Ocean response to a warmer world: insights from Marine Isotope Stage 5e,  
634 *Paleoceanography* 28, 1–14, doi:10.1002/palo.20052. 2013.

635 Cramer, B. S., Miller, K. G., Barrett, P. J., Wright, J. D.: Late Cretaceous-Neogene trends in  
636 deep ocean temperature and continental ice volume: Reconciling records of benthic  
637 foraminiferal geochemistry ( $\delta^{18}\text{O}$  and Mg/Ca) with sea level history, *Journal of Geophysical*  
638 *Research - Oceans* 116, C12023, 2011.

639 Creech, J. B., Baker, J. A., Hollis, C. J., Morgans, H. E. G. and Smith, E. G. C.: Eocene sea  
640 temperatures for the mid-latitude southwest Pacific from Mg/Ca ratios in planktonic and  
641 benthic foraminifera, *Earth and planetary science letters* 299(3/4), 483-495;  
642 doi:410.1016/j.epsl.2010.1009.1039, 2010.

643 Crouch, E. M., Heilmann-Clausen, C., Brinkhuis, H., Morgans, H. E. G., Egger, H., Schmitz,  
644 B.: Global dinoflagellate event associated with the late Paleocene thermal maximum,  
645 *Geology* 29, 315-318, 2001.

646 Crouch, E. M., Dickens, G. R., Brinkhuis, H., Aubry, M. P., Hollis, C. J., Rogers, K. M. and  
647 Visscher, H.: The *Apectodinium* acme and terrestrial discharge during the Paleocene-Eocene  
648 thermal maximum : new palynological, geochemical and calcareous nannoplankton  
649 observations at Tawanui, New Zealand, *Palaeogeography, palaeoclimatology, palaeoecology*  
650 194(4), 387-403, 2003.

651 Dickens, G. R.: Rethinking the global carbon cycle with a large, dynamic and microbially  
652 mediated gas hydrate capacitor, *Earth and Planetary Science Letters* 213, 169-183, 2003.

653 Dickens, G. R.: Down the Rabbit Hole: toward appropriate discussion of methane release  
654 from gas hydrate systems during the Paleocene-Eocene thermal maximum and other past  
655 hyperthermal events, *Clim. Past* 7, 831-846, 2011.

656 Dickens, G. R., Castillo, M. M., Walker, J. C. G.: A blast of gas in the latest Paleocene:  
657 Simulating first-order effects of massive dissociation of oceanic methane hydrate, *Geology*  
658 25, 259-262, 1997.

659 Dickens, G. R., O'Neil, J. R., Rea, D. K. and Owen, R. M.: Dissociation of oceanic methane  
660 hydrate as a cause of the carbon isotope excursion at the end of the Paleocene,  
661 *Paleoceanography* 10, 965-972, 1995.

662 Dunkley Jones, T., Lunt, D.J., Schmidt, D. N., Ridgwell, A., Sluijs, A., Valdes, P. J., and  
663 Maslin, M.: Climate model and proxy data constraints on ocean warming across the  
664 Paleocene–Eocene Thermal Maximum, *Earth Sci. Rev.*, 125, 123-145, doi:  
665 10.1016/j.earscirev.2013.07.004, 2013.

666 Eggins, S., De Deckker, P. and Marshall, J.: Mg/Ca variation in planktonic foraminifera tests:  
667 implications for reconstructing palaeo-seawater temperature and habitat migration, *Earth and*  
668 *Planetary Science Letters* 212, 291-306, doi:210.1016/S0012-1821X(1003)00283-00288,  
669 2003.

670 Evans, D. and Müller, W.: Deep time foraminifera Mg/Ca paleothermometry: Nonlinear  
671 correction for secular change in seawater Mg/Ca, *Paleoceanography* 27, PA4205, 2012.

672 Frieling, J., Iakovleva, A. I., Reichart, G. -J., Aleksandrova, G. N., Gribidenko, Z. N.,  
673 Schouten, S. and Sluijs, A.: Paleocene–Eocene warming and biotic response in the  
674 epicontinental West Siberian Sea, *Geology* 42, 767-770, 2014.

675 Gradstein, F. M., Ogg, J.G., Schmitz, M. and Ogg, G.: *The Geologic Time Scale 2012*,  
676 Elsevier Science BV, Oxford, UK, 2012.

677 Greaves, M., Barker, S., Daunt, C. and Elderfield, H.: Accuracy, standardization, and  
678 interlaboratory calibration standards for foraminiferal Mg/Ca thermometry, *Geochemistry,*  
679 *Geophysics, Geosystems* 6, doi:10.1029/2004GC000790, 2005.

680 Hancock, H. J. L., Dickens, G. R., Strong, C. P., Hollis, C. J. and Field, B. D.: Foraminiferal  
681 and carbon isotope stratigraphy through the Paleocene-Eocene transition at Dee Stream,  
682 Marlborough, New Zealand, *New Zealand Journal of Geology and Geophysics* 46, 1-19,  
683 2003.

684 Handley, L., Crouch, E. M. and Pancost, R. D.: A New Zealand record of sea level rise and  
685 environmental change during the Paleocene-Eocene Thermal Maximum, *Palaeogeography,*  
686 *Palaeoclimatology, Palaeoecology* 305, 185-200, 2011.

687 Hasiuk, F. J. and Lohmann, K. C.: Application of calcite Mg partitioning functions to the  
688 reconstruction of paleocean Mg/Ca, *Geochimica et Cosmochimica Acta* 74, 6751-6763, 2010.

689 Higgins, J. A. and Schrag, D. P.: Beyond methane: Towards a theory for the Paleocene-  
690 Eocene Thermal Maximum, *Earth and Planetary Science Letters* 245, 523-537, 2006.

691 Hollis, C. J.: Radiolarian faunal change across the Paleocene-Eocene boundary at Mead  
692 Stream, New Zealand, *Eclogae Geologicae Helvetiae* 99, S79-S99, 2006.

693 Hollis, C. J., Dickens, G. R., Field, B. D., Jones, C. J. and Strong, C. P.: The Paleocene-  
694 Eocene transition at Mead Stream, New Zealand: a southern Pacific record of early Cenozoic  
695 global change, *Palaeogeography, Palaeoclimatology, Palaeoecology* 215, 313-343, 2005a.

696 Hollis, C. J., Field, B. D., Jones, C. M., Strong, C. P., Wilson, G. J. and Dickens, G. R.:  
697 Biostratigraphy and carbon isotope stratigraphy of uppermost Cretaceous-lower Cenozoic in  
698 middle Clarence valley, New Zealand, *Journal of the Royal Society of New Zealand* 35, 345-  
699 383, 2005b.

700 Hollis, C.J., Taylor, K.W.T., Handley, L., Pancost, R.D., Huber, M., Creech, J., Hines, B.,  
701 Crouch, E.M., Morgans, H.E.G., Crampton, J.S., Gibbs, S., Pearson, P. and Zachos, J.C.:  
702 Early Paleogene temperature history of the Southwest Pacific Ocean: reconciling proxies and  
703 models, *Earth and Planetary Science Letters* 349-350, 53-66, 2012.

704 Hollis, C. J., Waghorn, D. B., Strong, C. P. and Crouch, E.M.: Integrated Paleogene  
705 biostratigraphy of DSDP site 277 (Leg 29): foraminifera, calcareous nannofossils, Radiolaria,



706 and palynomorphs, Institute of Geological & Nuclear Sciences Science Report 97/7, 1-73,  
707 1997.

708 Hollis, C. J., Tayler, M. J. S., Andrew, B., Taylor, K. W., Lurcock, P., Bijl, P. K., Kulhanek,  
709 D. K., Crouch, E. M., Nelson, C. S., Pancost, R. D., Huber, M., Wilson, G. S., Ventura, G. T.,  
710 Crampton, J. S., Schiøler, P. and Phillips, A.: Organic-rich sedimentation in the South Pacific  
711 Ocean associated with Late Paleocene climatic cooling, *Earth-Science Reviews* 134, 81-97,  
712 2014.

713 Horita, J., Zimmermann, H. and Holland, H. D.: Chemical evolution of seawater during the  
714 Phanerozoic: Implications from the record of marine evaporites, *Geochimica et*  
715 *Cosmochimica Acta* 66, 3733-3756, 2002.

716 Hornibrook, N. de B.: New Zealand Cenozoic marine paleoclimates : a review based on the  
717 distribution of some shallow water and terrestrial biota, in: Tsuchi, R., Ingle, J.C. (Eds.),  
718 *Pacific Neogene: environment, evolution and events*, University of Tokyo Press, Tokyo, pp.  
719 83-106, 1992.

720 Hornibrook, N. deB., Brazier, R. C. and Strong, C. P.: Manual of New Zealand Permian to  
721 Pleistocene foraminiferal biostratigraphy, New Zealand Geological Survey Paleontological  
722 Bulletin 56, 175 pp., 1989.

723 Inglis, G. N., Farnsworth, A., Lunt, D., Foster, G. L., Hollis, C. J., Pagani, M., Jardine, P. E.,  
724 Pearson, P. N., Markwick, P., Galsworthy, A. M. J., Raynham, L., Taylor, K. W. R. and  
725 Pancost, R. D.: Descent towards the Icehouse: Eocene sea surface cooling inferred from  
726 GDGT distributions, *Paleoceanography* 30, doi: 10.1002/2014PA002723, 2015.

727 Jones, G. A. and Kaiteris, P.: A vacuum-gasometric technique for rapid and precise analysis  
728 of calcium carbonate in sediment and soils, *J. Sed. Pet.* 53, 655-660, 1983.

729 Joughin, I., Smith, B. E. and Medley, B.: Marine Ice Sheet Collapse Potentially Under Way  
730 for the Thwaites Glacier Basin, West Antarctica, *Science* 344, 735-738, 2014.

731 Kahn, A. and Aubry, M. -P.: Provincialism associated with the Paleocene/Eocene thermal  
732 maximum: temporal constraint, *Mar. Micropal.* 52, 117-131, 2004.

733 Kaiho, K., Arinobu, T., Ishiwatari, R., Morgans, H. E. G., Okada, H., Takeda, N., Tazaki, K.,  
734 Zhou, G., Kajiwara, Y., Matsumoto, R., Hirai, A., Niitsuma, N. and Wada, H.: Latest  
735 Paleocene benthic foraminiferal extinction and environmental changes at Tawanui, New  
736 Zealand, *Paleoceanography* 11, 447-465, 1996.

737 Katz, M. E., Katz, D. R., Wright, J. D., Miller, K. G., Pak, D. K., Shackleton, N. J. and  
738 Thomas, E.: Early Cenozoic benthic foraminiferal isotopes: Species reliability and  
739 interspecies correction factors, *Paleoceanography* 18 (2), 1024, doi: 10.1029/2002PA000798,  
740 2003.

741 Kennett, J. P. Houtz, R.E. et al.: Initial reports of the Deep Sea Drilling Project, volume 29.  
742 U.S. Govt Printing Office, Washington, 1197 pp., 1975.

743 Kennett, J. P.: Cenozoic evolution of Antarctic glaciation, the Circum-Antarctic Ocean, and  
744 their impact on global paleoceanography, *Journal of Geophysical Research* 82, 3843-3860,  
745 1977.

746 Kennett, J. P.: Paleoceanographic and biogeographic evolution of the Southern Ocean during  
747 the Cenozoic, and Cenozoic microfossil datums, *Palaeogeography, Palaeoclimatology,*  
748 *Palaeoecology* 31, 123-152, 1980.

749 Kent, D. V., Cramer, B. S., Lanci, L., Wang, D., Wright, J. D. and Van der Voo, R.: A case  
750 for a comet impact trigger for the Paleocene/Eocene thermal maximum and carbon isotope  
751 excursion, *Earth and Planetary Science Letters* 211, 13-26, 2003.

752 Kim, S. -T. and O'Neil, J. R.: Equilibrium and nonequilibrium oxygen isotope effects in  
753 synthetic carbonates, *Geochimica et Cosmochimica Acta* 61, 3461-3475, 1997.

754 Kim, J. -H., van der Meer, J., Schouten, S., Helmke, P., Willmott, V., Sangiorgi, F., Koç, N.,  
755 Hopmans, E. C. and Damsté, J. S. S.: New indices and calibrations derived from the  
756 distribution of crenarchaeal isoprenoid tetraether lipids: Implications for past sea surface  
757 temperature reconstructions, *Geochimica et Cosmochimica Acta* 74, 4639-4654, 2010.

758 Kozdon, R., Kelly, D. C., Kitajima, K., Strickland, A., Fournelle, J. H. and Valley, J. W.: In  
759 situ  $\delta^{18}\text{O}$  and Mg/Ca analyses of diagenetic and planktic foraminiferal calcite preserved in a

760 deep-sea record of the Paleocene-Eocene thermal maximum, *Paleoceanography* 28, 517-528,  
761 2013.

762 Lear, C. H., Rosenthal, Y. and Slowey, N.: Benthic foraminiferal Mg/Ca-paleothermometry:  
763 a revised core-top calibration, *Geochimica et Cosmochimica Acta* 66, 3375-3387, 2002.

764 Liu, Z., Pagani, M., Zinniker, D., DeConto, R., Huber, M., Brinkhuis, H., Shah, S. R., Leckie,  
765 R. M. and Pearson, A.: Global Cooling During the Eocene-Oligocene Climate Transition,  
766 *Science* 323, 1187-1190, 2009.

767 Martini, E.: Standard Paleogene calcareous nannoplankton zonation, *Nature* 226, 560–561,  
768 1970.

769 Martini, E.: Standard Tertiary and Quaternary calcareous nannoplankton zonation, in:  
770 Farinacci, A. (Ed.), *Proceedings of the Planktonic Conference II*, Roma, 1970. Edizioni  
771 Tecnoscienze, Rome, 739–785, 1971.

772 McInerney, F. A. and Wing, S. L.: The Paleocene-Eocene Thermal Maximum: A  
773 Perturbation of Carbon Cycle, Climate, and Biosphere with Implications for the Future,  
774 *Annual Review of Earth and Planetary Sciences* 39, 489-516, 2011.

775 Nelson, C. S. and Cooke, P. J.: History of oceanic front development in the New Zealand  
776 sector of the Southern Ocean during the Cenozoic: a synthesis, *N.Z. J Geol. and Geophys.*  
777 44(4), 535-553, 2001.

778 Nicolo, M. J., Dickens, G. R., Hollis, C. J. and Zachos, J. C.: Multiple early Eocene  
779 hyperthermals: their sedimentary expression on the New Zealand continental margin and in  
780 the deep sea, *Geology* 35(8), 699-702; doi:610.1130/G23648A.23641, 2007.

781 Nicolo, M. J., Dickens, G. R. and Hollis, C. J.: South Pacific intermediate water oxygen  
782 depletion at the onset of the Paleocene-Eocene thermal maximum as depicted in New  
783 Zealand margin sections. *Paleoceanography* 25, PA4210, doi:4210.1029/2009PA001904,  
784 2010.

785 Norris, R. D., Wilson, P. A., Blum, P., and Expedition 342 Scientists: *Proceedings of the*  
786 *IODP*, 342, doi:10.2204/iodp.proc.2342.2014, 2014.

787 Nunes, F. and Norris, R. D.: Abrupt reversal in ocean overturning during the  
788 Palaeocene/Eocene warm period, *Nature (London)* 439, 60-63, 2006.

789 Olsson, R. K., Hemleben, C., Berggren, W. A. and Huber, B. T.: Atlas of Paleocene  
790 planktonic Foraminifera, *Smithsonian Contributions to Paleobiology* 85, 252 pp., 1999.

791 Oomori, T., H. Kaneshima, Y. Maezato, and Kitano, Y.: Distribution coefficient of  $Mg^{2+}$   
792 ions between calcite and solution at 10–50°C, *Marine Chemistry*, 20, 327–336, 1987.

793 Pearson, P. N. and Burgess, C. E.: Foraminifer test preservation and diagenesis: comparison  
794 of high latitude Eocene sites, *Geological Society, London, Special Publications* 303(1), 59-  
795 72, 2008.

796 Pearson, P. N., Olsson, R. K., Huber, B. T., Hemleben, C. and Berggren, W. A., 2006. Atlas  
797 of Eocene Planktonic Foraminifera, *Cushman Foundation Special Publication* no. 41, 514 p,  
798 2006.

799 Pearson, P. N., van Dongen, B. E., Nicholas, C. J., Pancost, R. D., Schouten, S., Singano, J.  
800 M. and Wade, B. S.: Stable warm tropical climate through the Eocene Epoch, *Geology* 35,  
801 211-214, 2007.

802 Perch-Nielsen, K.: Cenozoic calcareous nannofossils, in: Bolli, H.M., Saunders, J. B. and  
803 Perch-Nielsen, K. (Eds.), *Plankton Stratigraphy*. Cambridge University Press, Cambridge,  
804 427–554. 1985.

805 Quillévéré, F. and Norris, R. D.: Ecological development of acarininids (planktonic  
806 foraminifera) and hydrographic evolution of Paleocene surface waters, *GSA Special Papers*  
807 369, 223-238, 2003.

808 Raine, J. I., Beu, A. G., Boyes, A. F., Campbell, H. J., Cooper, R. A., Crampton, J. S.,  
809 Crundwell, M. P., Hollis, C. J. and Morgans, H. E. G.: Revised calibration of the New  
810 Zealand Geological Timescale: NZGT2015/1, *GNS Science Report* 2012/39, 1-53, 2015.

811 Raffi, I. and De Bernardi, B.: Response of calcareous nannofossils to the Paleocene–Eocene  
812 Thermal Maximum: Observations on composition, preservation and calcification in

813 sediments from ODP Site 1263 (Walvis Ridge—SW Atlantic), *Mar. Micropal.* 69, 119-138,  
814 2008.

815 Rampino, M.R.: Peraluminous igneous rocks as an indicator of thermogenic methane release  
816 from the North Atlantic Volcanic Province at the time of the Paleocene–Eocene Thermal  
817 Maximum (PETM), *Bulletin of Volcanology* 75, 1-5, 2013.

818 Richter, T. O., van der Gaast, S., Kaster, B., Vaars, A., Gieles, R., de Stigter, H. C., De Haas,  
819 H. and van Weering, T. C. E.: The Avaatech XRF core scanner: technical description and  
820 applications to NE Atlantic sediments, Geological Society of London, Special Publications  
821 267, 39–50. doi:10.1144/GSL.SP.2006.267.01.03, 2006.

822 Röhl, U., Westerhold, T., Bralower, T. J. and Zachos, J. C.: On the duration of the Paleocene-  
823 Eocene thermal maximum (PETM), *Geochemistry, Geophysics, Geosystems* 8, doi:  
824 10.1029/2007GC001784, 2007.

825 Schmidt, G. A., Annan, J. D., Bartlein, P. J., Cook, B. I., Guilyardi, E., Hargreaves, J. C.,  
826 Harrison, S. P., Kageyama, M., LeGrande, A. N., Konecky, B., Lovejoy, S., Mann, M. E.,  
827 Masson-Delmotte, V., Risi, C., Thompson, D., Timmermann, A., Tremblay, L. B., and Yiou,  
828 P.: Using palaeo-climate comparisons to constrain future projections in CMIP5, *Clim. Past*  
829 10, 221-250, doi: 10.5194/cp-10-221-2014, 2014.

830 Schrag, D. P.: Effect of diagenesis on the isotopic record of late Paleogene tropical sea  
831 surface temperatures, *Chemical Geology* 161, 215-224, 1999.

832 Schrag, D. P., DePaolo, D. J. and Richter, F. M.: Reconstructing past sea surface  
833 temperatures: Correcting for diagenesis of bulk marine carbonate, *Geochimica et*  
834 *Cosmochimica Acta* 59, 2265-2278.

835 Schweizer, M., Pawlowski, J., Kouwenhoven, T. and van der Zwaan, B.: Molecular  
836 phylogeny of common cibicidids and related Rotaliida (Foraminifera) based on small subunit  
837 rDNA sequences, *The Journal of Foraminiferal Research* 39, 300-315, 2009.

838 Sexton, P. F., Wilson, P. A. and Pearson, P. N.: Microstructural and geochemical  
839 perspectives on planktic foraminiferal preservation: “Glassy” versus “Frosty”, *Geochemistry,*  
840 *Geophysics, Geosystems - G<sup>3</sup> 7*, doi: 10.1029/2006GC001291, 2006.

841 Shackleton, N. J. and Kennett, J. P.: Paleotemperature history of the Cenozoic and the  
842 initiation of Antarctic glaciation : oxygen and carbon isotope analyses in DSDP sites 277,  
843 279, and 281, Initial reports of the Deep Sea Drilling Project 29, 743-755, 1975.

844 Slotnick, B. S., Dickens, G. R., Nicolo, M., Hollis, C. J., Crampton, J. S., Zachos, J. C. and  
845 Sluijs, A.: Numerous large amplitude variations in carbon cycling and terrestrial weathering  
846 throughout the latest Paleocene and earliest Eocene, *Journal of Geology* 120, 487-505, 2012.

847 Sluijs, A., Bowen, G., Brinkhuis, H., Lourens, L. and Thomas, E.: The Palaeocene-Eocene  
848 Thermal Maximum super greenhouse: biotic and geochemical signatures, age models and  
849 mechanisms of global change, in: Williams, M. et al. (Eds.), *Deep time perspectives on*  
850 *climate change: marrying the signal from computer models and biological proxies*, The  
851 *Geological Society of London, Special Publication*, pp. 323-347, 2007.

852 Sluijs, A., Bijl, P. K., Schouten, S., Roehl, U., Reichart, G. J. and Brinkhuis, H.: Southern  
853 ocean warming, sea level and hydrological change during the Paleocene-Eocene thermal  
854 maximum, *Clim. Past* 7, 47-61, 2011.

855 Stanley, S. M. and Hardie, L. A.: Secular oscillations in the carbonate mineralogy of reef-  
856 building and sediment-producing organisms driven by tectonically forced shifts in seawater  
857 chemistry, *Palaeogeography, Palaeoclimatology, Palaeoecology* 144, 3-19, 1998.

858 Stoll, H.M.: Limited range of interspecific vital effects in coccolith stable isotopic records  
859 during the Paleocene-Eocene thermal maximum, *Paleoceanography* 20, doi:  
860 10.1029/2004PA001046, 2005.

861 Svensen, H.: Release of methane from a volcanic basin as a mechanism for initial Eocene  
862 global warming, *Nature* 429, 542-545, 2004.

863 Taylor, K. W. R., Huber, M., Hollis, C. J., Hernandez-Sanchez, M. T. and Pancost, R. D.: Re-  
864 evaluating modern and Palaeogene GDGT distributions: Implications for SST  
865 reconstructions, *Global and Planetary Change* 108, 158-174, 2013.

866 Tierney, J. E. and Tingley, M. P.: . A Bayesian, spatially-varying calibration model for the  
867 TEX<sub>86</sub> proxy, *Geochimica et Cosmochimica Acta* 127, 83-106, 2014.

868 Villasante-Marcos, V., Hollis, C. J., Dickens, G. R. and Nicolo, M. J.: Rock magnetic  
869 properties across the Paleocene-Eocene Thermal Maximum in Marlborough, New Zealand,  
870 *Geologica Acta* 7(1/2), 229-242, 2009.

871 Wilkinson, B. H. and Algeo, T. J.: The sedimentary carbonate record of calcium magnesium  
872 cycling, *American Journal of Science* 289, 1158-1194, 1989.

873 Zachos, J. C., Stott, L. D. and Lohmann, K. C., 1994. Evolution of early Cenozoic marine  
874 temperatures, *Paleoceanography* 9, 353-387, 1994.

875 Zachos, J. C., Pagani, M., Sloan, L. C., Thomas, E. and Billups, K.: Trends, rhythms, and  
876 aberrations in global climate 65 Ma to present, *Science* 292, 686-693, 2001.

877 Zachos, J. C., Wara, M. W., Bohaty, S., Delaney, M. L., Petrizzo, M. R., Brill, A., Bralower,  
878 T. J. and Premoli-Silva, I., 2003. A transient rise in tropical sea surface temperature during  
879 the Paleocene-Eocene thermal maximum, *Science* 302, 1551-1554, 2003.

880 Zachos, J. C., Röhl, U., Schellenberg, S. A., Sluijs, A., Hodell, D. A., Kelly, D. C., Thomas,  
881 E., Nicolo, M., Raffi, I., Lourens, L. J., McCarren, H. and Kroon, D. : Rapid acidification of  
882 the ocean during the Paleocene-Eocene Thermal Maximum, *Science* 308, 1611-1615, 2005.

883 Zachos, J. C., Schouten, S., Bohaty, S., Quattlebaum, T., Sluijs, A., Brinkhuis, H., Gibbs, S.  
884 J. and Bralower, T. J.: Extreme warming of mid-latitude coastal ocean during the Paleocene-  
885 Eocene Thermal Maximum: Inferences from TEX<sub>86</sub> and isotope data., *Geology* 34, 737-740,  
886 2006.

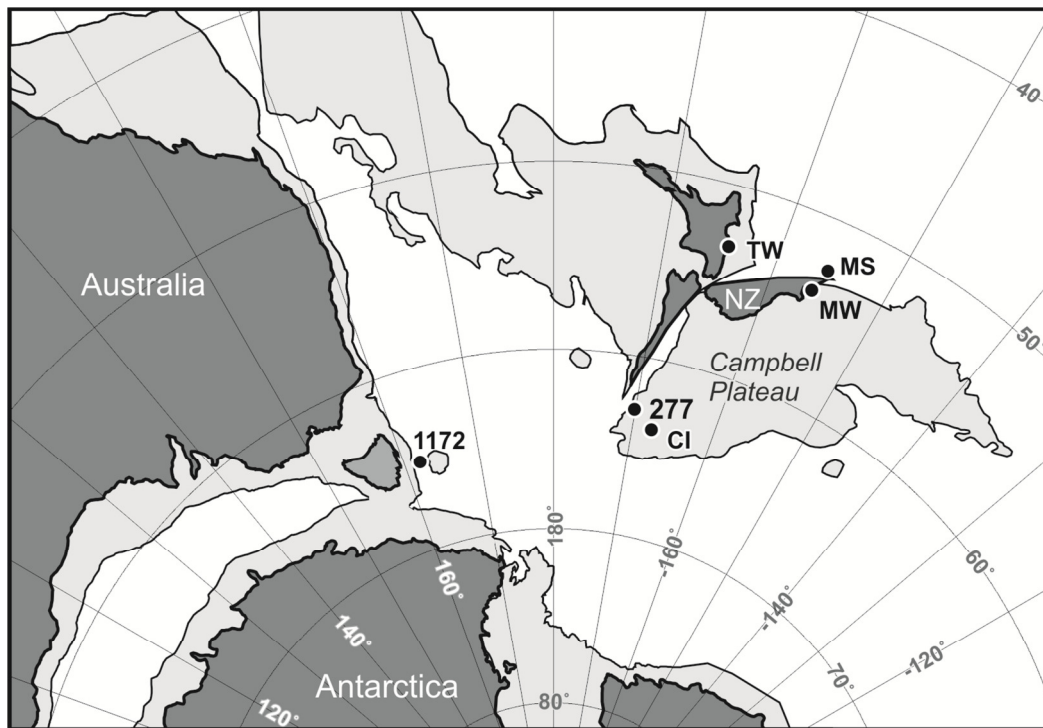
887 Zachos, J. C., Dickens, G. R. and Zeebe, R. E.: An early Cenozoic perspective on greenhouse  
888 warming and carbon-cycle dynamics, *Nature* 451, 279-283, 2008.

889 Zachos, J. C., McCarren, H., Murphy, B., Röhl, U. and Westerhold, T.: Tempo and scale of  
890 late Paleocene and early Eocene carbon isotope cycles: Implications for the origin of  
891 hyperthermals, Earth and Planetary Science Letters 299, 242-249, 2010.

892

893

894

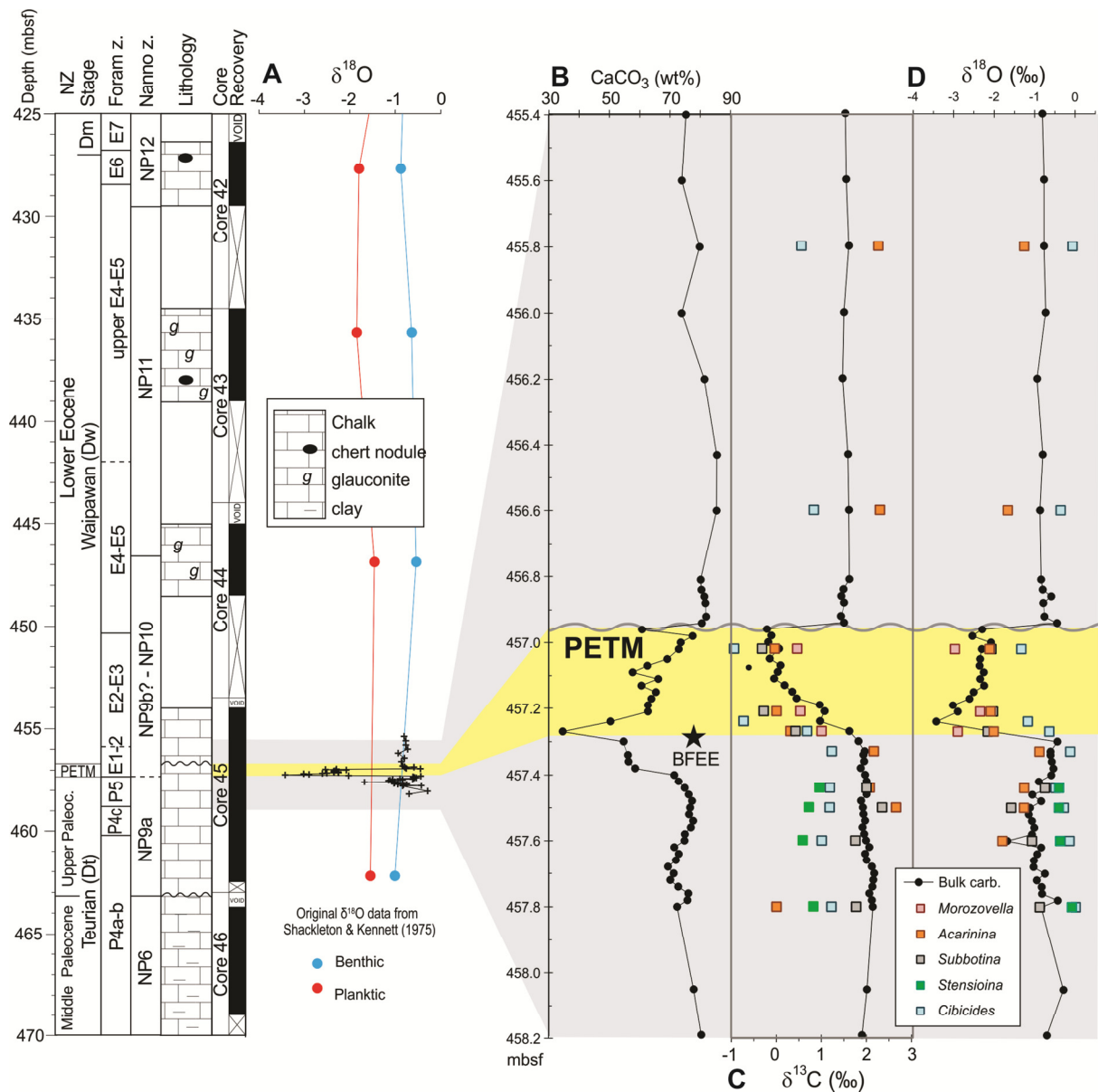


895

896 Figure 1. Location of DSDP Site 277 on a tectonic reconstruction for the southwest Pacific  
897 during the early Eocene (~54 Ma) (after Cande and Stock, 2004). Other localities mentioned  
898 in the text are also shown: ODP Site 1172, Campbell Island (CI), Tawanui (TW), Mid-  
899 Waipara River (MW) and Mead Stream (MS).

900

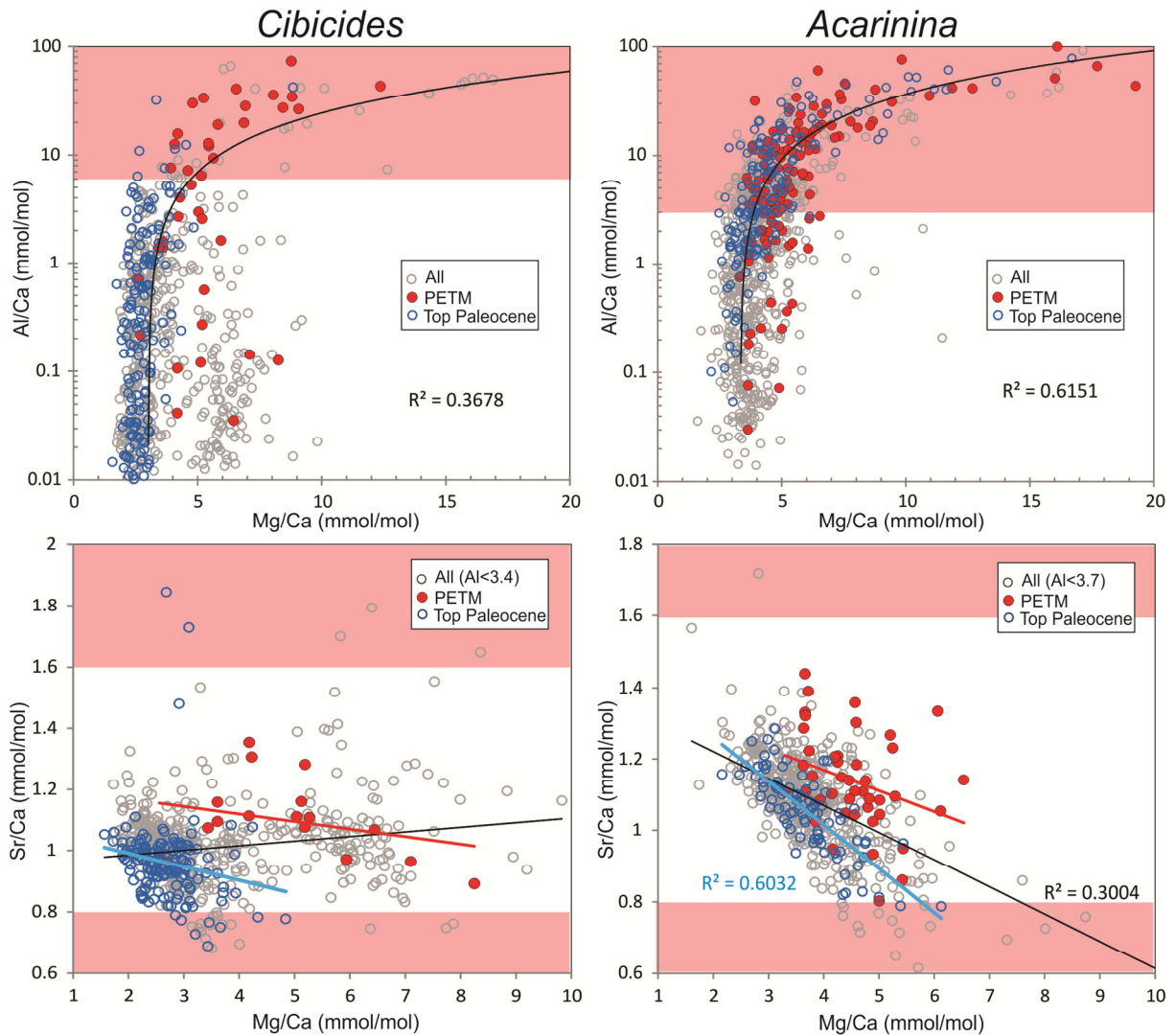




901

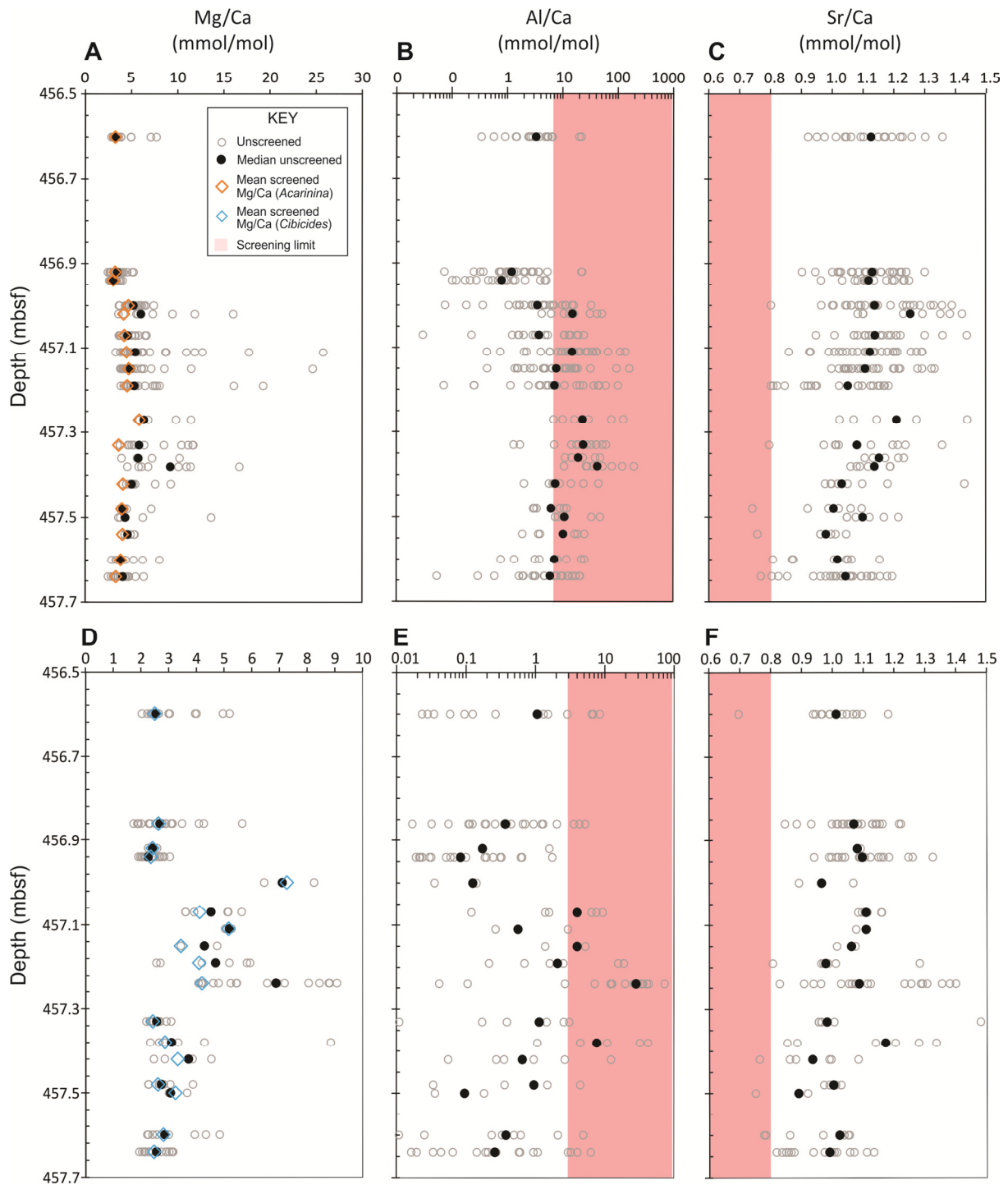
902 Figure 2. Biostratigraphy, lithologies, carbonate content (B) and stable isotopes from bulk  
 903 carbonate and foraminifera (A, C, D) across the Paleocene-Eocene transition at DSDP Site  
 904 277. Abbreviations: Mangaorapan local stage (Dm); Paleocene Eocene Thermal Maximum  
 905 (PETM), Benthic Foraminiferal Extinction Event (BFEE). In (A) the new bulk carbonate  
 906  $\delta^{18}\text{O}$  record is plotted alongside the uncorrected, mixed planktic and benthic  $\delta^{18}\text{O}$  values of  
 907 Shackleton and Kennett (1975); in (D) and subsequent figures, benthic  $\delta^{18}\text{O}$  values include a  
 908 correction factor of 0.28‰ (Katz et al., 2003).

909



910

911 Figure 3. Cross-plots of Mg/Ca, Al/Ca and Sr/Ca with areas outside the screening limit  
 912 shaded pink. All results are shown for the Al/Ca–Mg/Ca cross plots. For Sr/Ca–Mg/Ca cross  
 913 plots, we only include measurements that lies within the screening limit for Al/Ca in order to  
 914 exclude the effects of silicate contamination. Only  $R^2$  values significant at the 95%  
 915 confidence interval are shown for the trend lines.

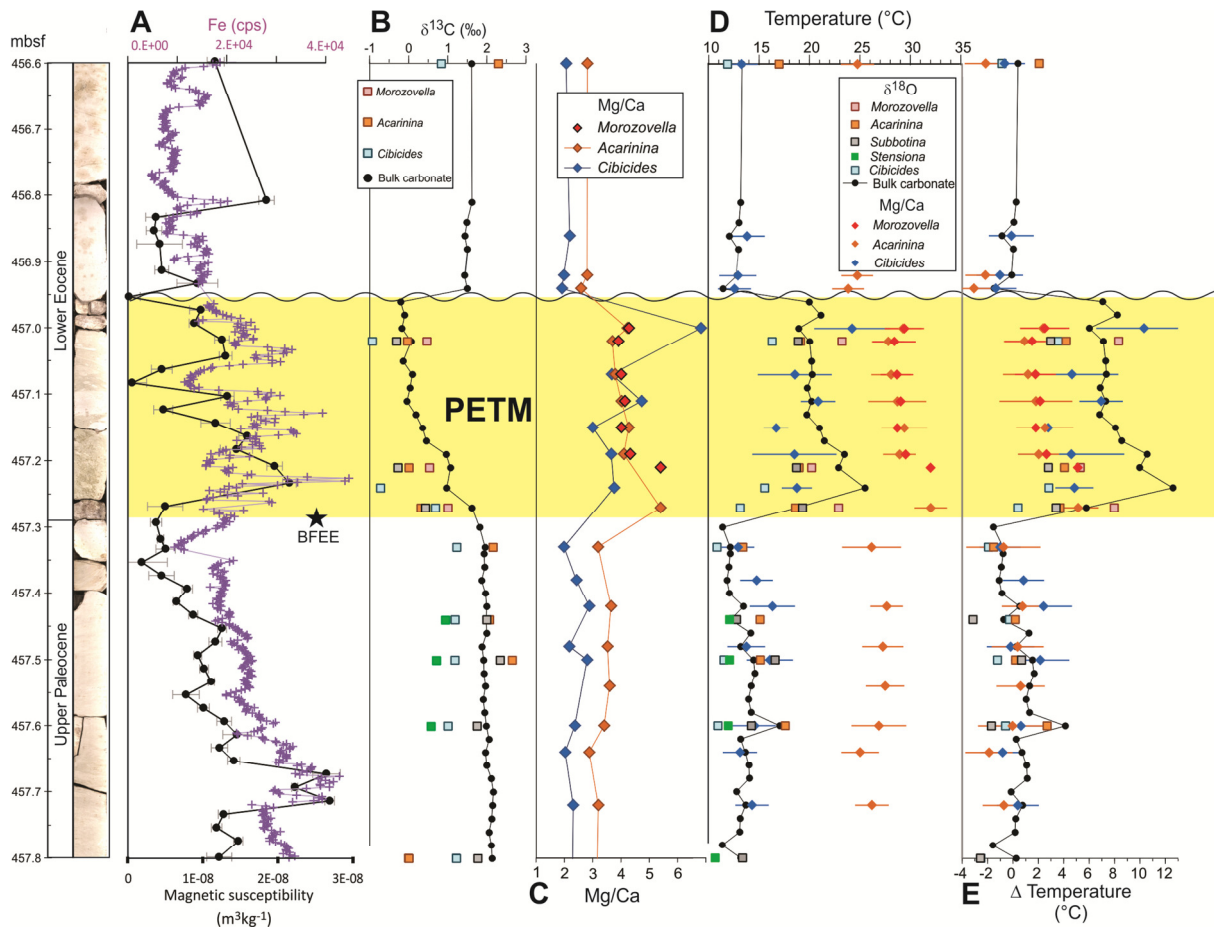


916

917

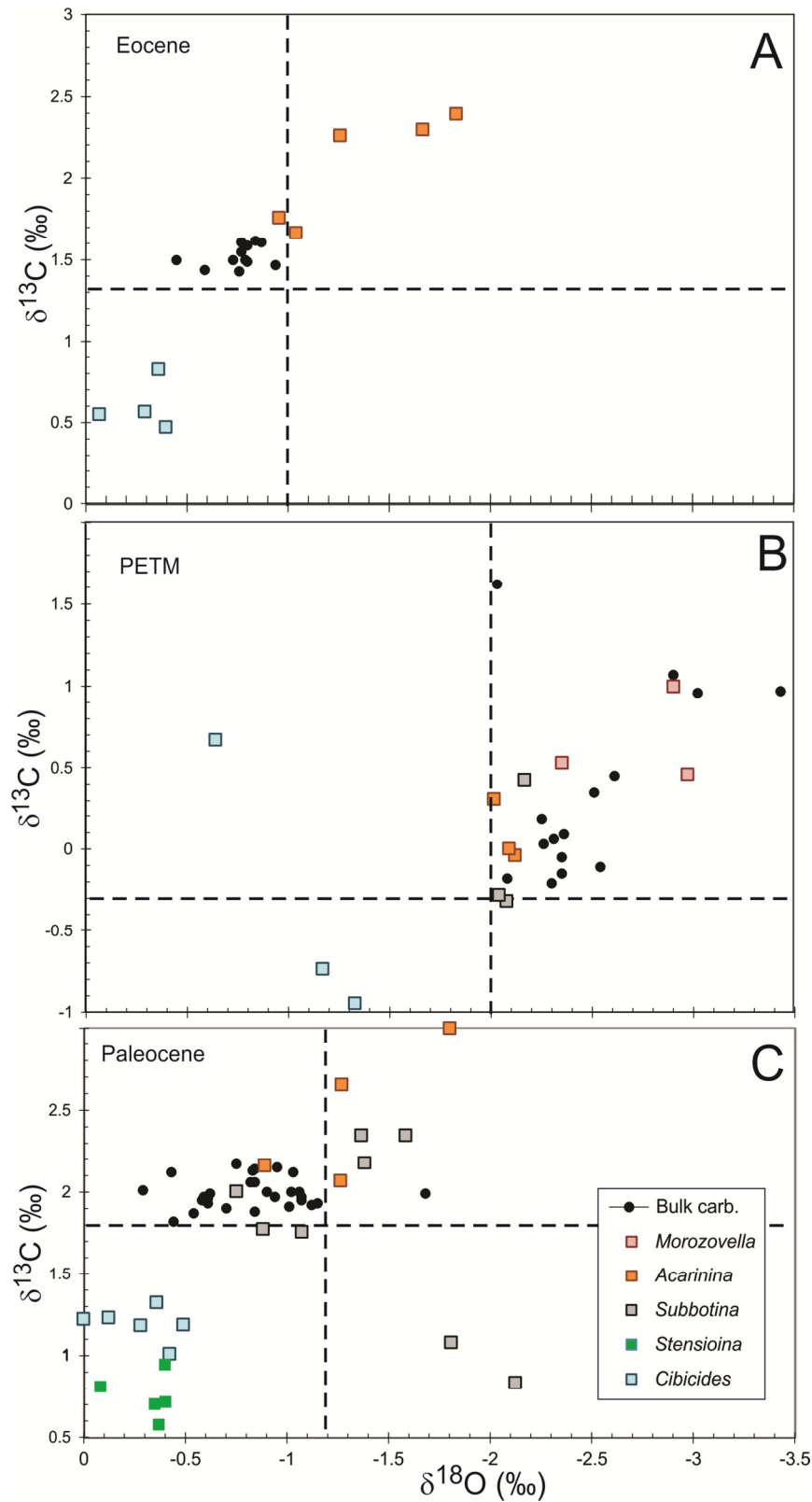
918 Figure 4. Trace element–depth plots for *Acarinina* (A–C) and *Cibicides* (D–F) across the  
 919 PETM interval, showing all measured Mg/Ca, Al/Ca and Sr/Ca values, and the decrease in  
 920 mean Mg/Ca value when Al/Ca and Sr/Ca screening protocols are imposed. Areas outside  
 921 the screening limits are shaded pink. Note change in scale on horizontal axes for Mg/Ca and  
 922 Al/Ca for *Acarinina* and *Cibicides*.

923



924  
 925  
 926  
 927  
 928  
 929  
 930

Figure 5. Variation in (A) Fe content and magnetic susceptibility; (B)  $\delta^{13}\text{C}$ ; (C) Mg/Ca ratios; (D) paleotemperatures derived from  $\delta^{18}\text{O}$  values and Mg/Ca ratios; and (E) changes in paleotemperature relative to average Paleocene values.



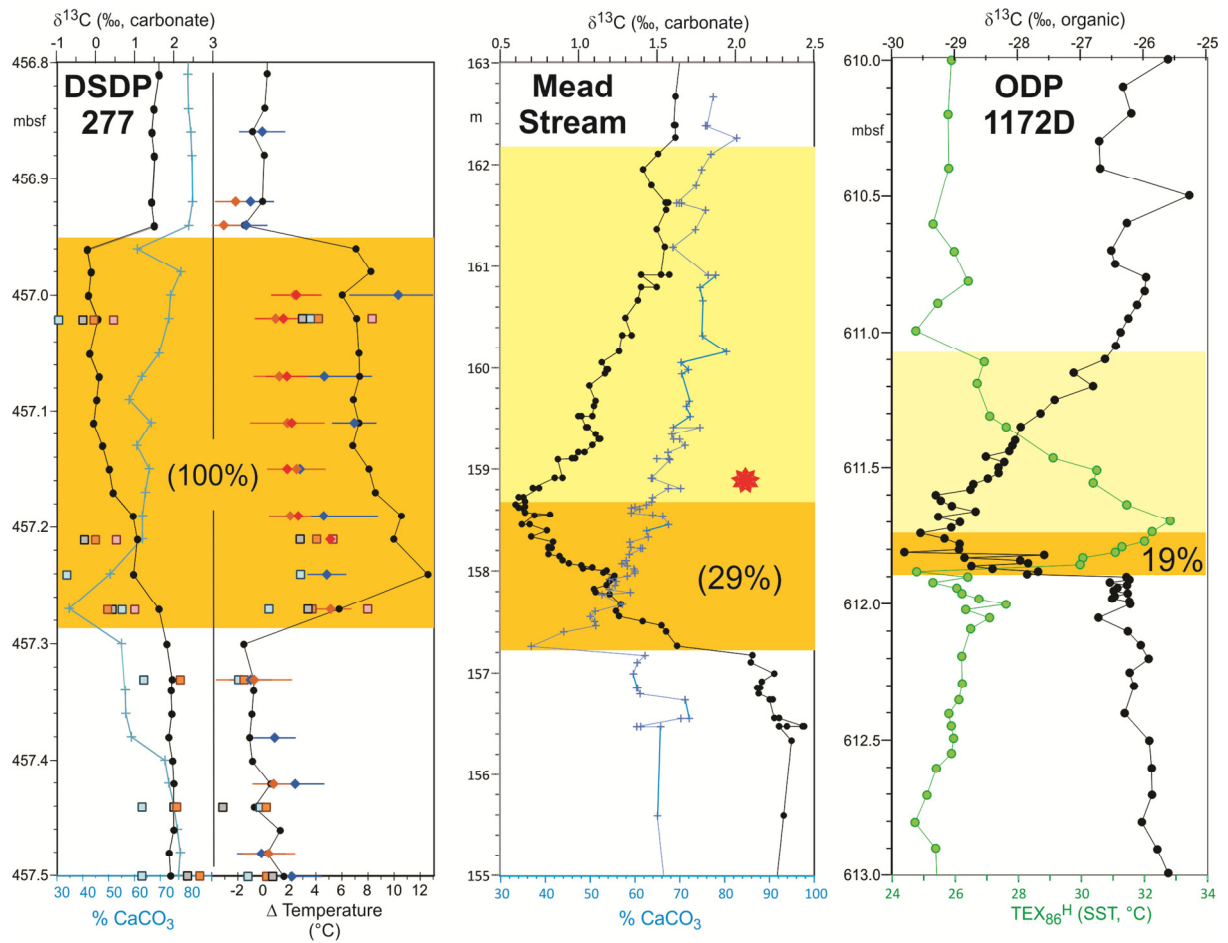
931

932

933 Figure 6. Cross plot of stable isotope ( $\delta^{13}\text{C}$ ,  $\delta^{18}\text{O}$ ) values for bulk carbonate, *Cibicides*,

934 *Acarinina* and *Morozovella* within the Paleocene, Paleocene Eocene Thermal Maximum

935 (PETM), and overlying Eocene.



936

937 Figure 7. Comparison of records of the Paleocene–Eocene thermal maximum (PETM) at  
 938 DSDP Site 277, ODP Site 1172 and Mead Stream. Symbols for DSDP Site 277 as in Fig. 4.  
 939 Note the bulk carbonate  $\delta^{18}\text{O}$  record is not plotted as a guide for relative temperature change  
 940 at DSDP 277 because the record is inferred to be affected by diagenesis. The Red star marks  
 941 a single occurrence of low-latitude radiolarians in the P-E transition interval at Mead Stream  
 942 (Hollis, 2006).

943